*Original Article*

# Seismic response control of building structures under pulse-type ground motions by active vibration controller

Said Elias[1,2] , Salah Djerouni[1,3], Dario De Domenico[4], Mahdi Abdeddaim[3]  and Mohamed Hechmi El Ouni[5]

## Abstract

Active vibration control systems are commonly reported to be the most robust and effective method for vibration control of structures. However, the type of ground motions and the type of analysis may greatly influence their performances. This study investigates the seismic response of building with and without an active controller under pulse-type ground motions. A 20-story non-linear steel benchmark building is considered. Linear and non-linear analysis is conducted to check the effectiveness of the active control system. Active control with a linear quadratic Gaussian (LQG) control algorithm is applied to the benchmark building for seismic control purposes. Initially, some ground motions are selected following earlier studies from the literature concerning the benchmark building. It is found that the LQG control algorithm is quite effective under the considered earthquakes, and the analysis type does not affect the effectiveness of the controller. Thereafter, a set of additional 69 pulse-type ground motions are considered to check the performance of the LQG control algorithm and to find the suitability of linear analysis. It is noticed that under such pulse-type ground motion, the LQG control algorithm is not much effective if the non-linear behavior of the structure is incorporated in the seismic analysis, whereas in case of linear analysis, the LQG control algorithm is still effective. It is concluded that neglecting the non-linear behavior may lead to unconservative estimates of the seismic response when performing seismic analysis and designing structures equipped with active vibration control systems.

## Keywords

## Introduction

Vibration control of structures is developing quite fast, and till date, various methods such as passive, semi-active, hybrid, and active have been presented by researchers. Although passive systems are the simplest and cheapest system[1]; the other three schemes are considered extra safety, especially for structures with important social and economic value (e.g., hospitals, schools, power plants, etc.). Many literature studies focused on using active and semi-active control systems for seismic response control; here, only a few recent papers are mentioned for brevity purposes. Amjadian[2] showed that friction

[1]Earthquake Engineering Research Centre, Faculty of Civil and Environmental Engineering, School of Engineering and Natural Sciences, University of Iceland, Selfoss, Iceland
[2]Department of Construction Management and Engineering (CME), Faculty of Engineering Technology (ET), University of Twente (UTWENTE), Enschede, Netherlands
[3]Laboratory of Research in Civil Engineering, Hydraulics, Sustainable Development and Environment, Faculty of Science and Technology, University Mohamed Khider Biskra, Biskra, Algeria
[4]Department of Engineering, University of Messina, Messina, Italy
[5]Department of Civil Engineering, College of Engineering, King Khalid University, Abha, Saudi Arabia

**Corresponding author:**
Said Elias, Earthquake Engineering Research Centre (EERC), University of Iceland, Austurvegur 2A 800 Selfoss, Selfoss 800, Iceland.
Email: elias.rahimi@utwente.nl

dampers are the most reliable devices of energy dissipation. Amjadian and Agrawal[3] used smart electromagnetic friction damper for response control of base-isolated buildings. Soto and Adeli[4] reported that semi-active control devices like magneto-rheological (MR) dampers could significantly increase the seismic performance of isolated structures. The use of MR dampers was investigated in many recent studies. Azar et al.[5] and Raeesi et al.[6] proposed a novel MR damper, which was found to provide very competitive results compared to other control algorithms. Zhao et al.[7] showed the performance of MR damper in response reduction of frame structures. Lu et al.[8,9] showed that the performance of the impact dampers, particle dampers, and semi-active particle dampers could be considerably improved by parameter optimization. Hormozabad and Soto[10] used artificial intelligence (AI) to optimize the MR damper parameters for seismic response control of structures. Saeed et al.[11] recently, proposed smart semi-active controllers using Brain Emotional Learning Based Intelligent Controller (BELBIC). It was found that the proposed self-tuned BELBIC (ST-BELBIC) effectively diminish the seismic responses of smart civil structure.

Yanik[12] and Yanik et al.[13,14] showed the performance of an active control system in response mitigation of structures. Moghaddasie and Jalaeefar[15] found that the optimum active system was more effective than the conventional system in the case of seismic response control. Ümütlü et al.[16] designed an active controller that reached the control aim showing inherent robustness, although it was tested only under four earthquake ground motions. An active integrated control system was proposed by Akyürek and Suksawang.[17] They showed that the proposed method was effective in response control of buildings under bidirectional ground motions.

Near-field ground motions with directivity effects tend to have a high peak ground velocity (PGV)/peak ground acceleration (PGA) ratio, which significantly affects their response characteristics.[18] Mazza[19] elegantly highlighted that the effects of near-field ground motions should be considered through appropriate further code provisions. Ghowsi and Sahoo[20,21] presented the performance of novel buckling restrained braces (BRBs) in response reduction of structures under near-field ground motions. Gentile and Galasso[22] found that the influence of near-source directivity can be reasonably neglected in the fragility derivation, particularly for rigid structures. Li et al.[23] showed the sliding mode controller's extremely high performance and robustness designed for the benchmark problem. Several researchers have shown different methods to select the ground motions for structural assessment and performance checks. Liu et al.[24] used modal based ground motion selection procedure to select ground motions for time-history analysis of tall buildings under earthquakes. Zhang et al.[25] used weighted and unweighted scaling methods for ground motion selection for non-linear analysis. In the case of near-field pulse-type ground motions, a method by Sigurðsson et al.[26] can be an effective way to select the ground motions.

## Motivation and outline of this study

While reviewing past studies, investigating the performance of active controllers for seismic control of building structures under pulse-type ground motions is essential. Therefore, the objective of this study is to present the performance of the active controller for the mitigation of vibrations caused by pulse-like ground motions. Therefore, in this study, the pulse-like ground motions are taken from the list given by Sigurðsson et al.[26]

Control actuators are positioned throughout the 20-story benchmark building's above-ground storeys, connecting adjacent levels. The actuators' size is restricted to offer maximum control forces of 1000 kN. This capacity of the actuator is widely available. Multiple actuators can give bigger control forces at a specific place. The control actuators for this sample control scheme are installed on each level of the structure, totalling 25 actuators for the 20-story benchmark building. The ground level has four actuators, the first and second levels have two actuators each, and the third through 20th levels of the structure have one actuator each. Each actuator is installed in the structure utilizing a chevron bracing arrangement, in which the actuator is horizontal and rigidly attached between the building's two levels. As a result, the first-level actuators will create equal and opposing control forces on the first and second levels. The compliance of the bracing is ignored in the study Ohtori et al.[27] and Wongprasert and Symans.[28]

The sample control method is based on acceleration feedback because accelerometers can easily give reliable and inexpensive measurements of absolute accelerations at any position on a structure. For feedback, the control system uses acceleration data from the 4th, 8th, 12th, 16th, and 20th floors. At these story levels, five sensors are employed to measure absolute accelerations Ozbulut and Hurlebaus[29] and Elias and Matsagar.[30]

## Mathematical modelling of non-linear benchmark building

In this study, a 20-story steel building[27] designed for the Structural Association of California (SAC) project for the Los Angeles, California region, is chosen to investigate the effect of pulse-like ground motions. The literature used this structure

as a non-linear/linear seismic control design benchmark. In the case of active control, a specific number of sensors are located in several building levels coupled to appropriate control algorithms (see Figure 1). Also, five sensors are placed while keeping the same distance between each sensor starting from the fourth level. The detail of the benchmark building is shown in Figure 1; it shows dimensions of 30.48 m × 36.58 m in plan and 80.77 m in elevation.

The lateral load resisting system of the building consists of two steel perimeter moment-resisting frames (MRFs) with a gravity frame in between. The total mass of the benchmark structure is equal to $1.11 \times 10^4$ tons. The first 10 natural frequencies of the 20-story benchmark building are summarized in Table 1. MATLAB Simulink (2019) has been selected for simulating the seismic response of the benchmark building. The second-order Dormand-Prince algorithm (solver) is utilized for solving the non-linear equation of motion. The SIMULINK block diagrams for the analysis of the benchmark building are illustrated in Figure 2. More detailed information of the benchmark building can be found in Ohtori et al.[27] This study aims to compare the effectiveness of active control for both linear and non-linear models while subjected to a set of 69 near-fault pulse-like ground motions.[26,31] Seismological details of these earthquake ground motions are listed in Table 2. Note that the information in the table is arranged properly from the lowest to the largest values of peak ground acceleration (PGA). The ground motions are obtained from earthquakes with a moment magnitude range [5.74–7.6]. The range of Joyner-Boore distance is [0–26.32 km], and that of peak ground acceleration (PGA) is [0.13–1.43] g, where g denotes the gravity acceleration. The interval of predominant periods of the selected ground motions is [0.58–9.78] s, and that of peak ground velocity (PGV) is [0.22–1.40] cm/s.
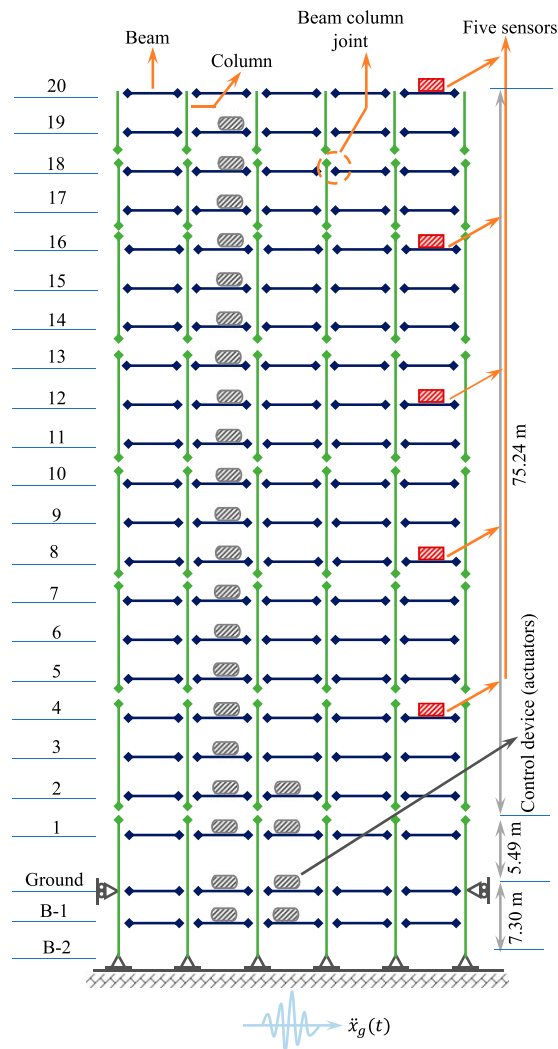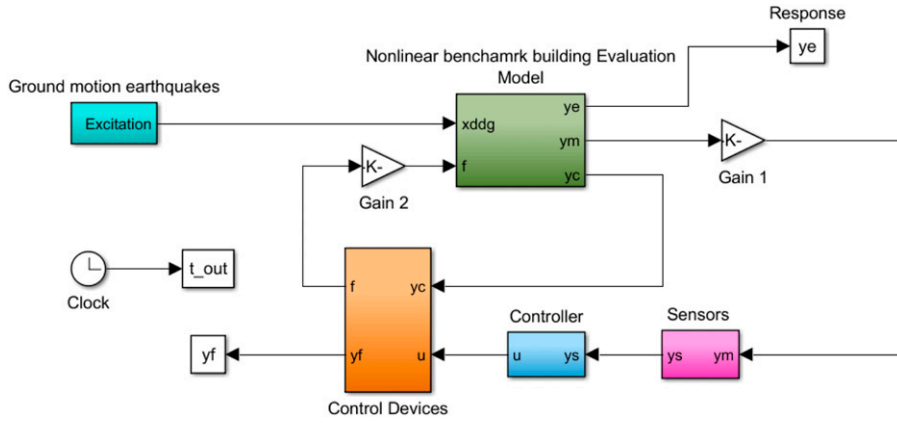


**Figure 1.** Twenty-story benchmark building.

**Table 1.** The first 10 natural frequencies of 20-story benchmark building.

| Mode | 1 | 2 | 3 | 4 | 5 | 6 | 7 | 8 | 9 | 10 |
|---|---|---|---|---|---|---|---|---|---|---|
| $f(Hz)$ | 0.261 | 0.753 | 1.30 | 1.83 | 2.40 | 2.44 | 2.92 | 3.01 | 3.63 | 3.68 |



**Figure 2.** Exhibit SIMULINK block diagram for a structural system.

The governing equation of motion of the structural system under horizontal seismic excitation is given in the following form:

$$[M_t]\{\ddot{x}_t\} + [C_t]\{\dot{x}_t\} + [K_t]\{x_t\} = \{F_G\} \tag{1}$$

where mass, damping, and stiffness matrices of the benchmark building are respectively denoted $[M_t]$, $[C_t]$, and $[K_t]$. Moreover $\{x_t\}$, $\{\dot{x}_t\}$, and $\{\ddot{x}_t\}$ are unknown displacement, velocity, and acceleration response vectors. The other term in the right side of equation (1) represents the force applied to the structural system defined as follows:

$$F_G = -[M_t]\{\Lambda\}\{\ddot{x}_g\} + \{P\}\{f\} + \{F_{err}\} \tag{2}$$

Herein, $\{\Lambda\}$ and $\{\ddot{x}_g\}$ are the influence vector and seismic ground acceleration vector, respectively. Further, $\{P\}$, $\{f\}$, and $\{F_{err}\}$ are the loading vector for the control force, a control force vector, and the vector of an unbalanced force, respectively. Moreover, this later unknown is the difference between the two restoring forces, which is evaluated as:

$$\{F_{err}\} = \{F_u\}_{NL} - \{F_u\}_L \tag{3}$$

Hence, $\{F_u\}_{NL}$ refers to the restoring force calculated using the non-linear hysteresis model and $\{F_u\}_L$ is the corresponding restoring force due to constant linear stiffness (the subscript NL, L denotes non-linear and linear state, respectively). The floor slabs are assumed to be stiff, thus assigning all the nodes the same horizontal displacement. Therefore, the number of degrees of freedom (DOFs) is reduced and entails only the effective nodes $x_{t,eff}$, including all vertical and rotational DOF plus one horizontal DOF per level.[27] If $x_{t,slv}$ is the original number of DOFs of benchmark building, the following relation can be written:

$$x_t = \{x_{t,eff} \quad x_{t,slv}\}^T = T_R x_{t,eff} \tag{4}$$

The relevant $[M_t]$ and $[K_t]$ matrices read

$$[M_t] = [T_R]^T[M_t][T_R], [K_t] = [T_R]^T[K_t][T_R] \tag{5}$$

where $[T_R]$ is the transformation matrix for expressing the full response vector in terms of effective DOFs, and superscript (T) denotes matrix transpose.

The damping matrix is determined based on Rayleigh damping theory as follows:

**Table 2.** Sixty-nine near-fault pulse-like ground motions considered in this study Elias et al.[31] and Azar et al.[5]

| Earthquake | Date | Station | Comp | $M$ | $R_{jb}$ (km) | $T$ (sec) | PGA (g) | PGV (cm/s) |
|---|---|---|---|---|---|---|---|---|
| Chi-Chi, Taiwan | 20-Sep-99 | TCU103 | SN | 7.6 | 6.1 | 7.2152 | 0.1323 | 62.5 |
| Izmit, Tukey | 17-Aug-99 | ARC | SN | 7.51 | 10.56 | 6.44 | 0.1331 | 44.3 |
| Chi-Chi, Taiwan | 20-Sep-99 | TCU036 | SN | 7.6 | 19.84 | 5.0845 | 0.1345 | 62.3 |
| Chi-Chi, Taiwan | 20-Sep-99 | TCU046 | SN | 7.6 | 16.74 | 6.7891 | 0.1394 | 44.33 |
| Chi-Chi, Taiwan | 20-Sep-99 | TCU038 | SN | 7.6 | 25.44 | 5.9202 | 0.1398 | 50.9 |
| Chi-Chi, Taiwan | 20-Sep-99 | TCU040 | SN | 7.6 | 22.08 | 5.6132 | 0.1452 | 53.2 |
| Parkfield, CA, USA | 28-Sep-04 | Parkfield fault zone 9 | SN | 6 | 1.25 | 1.0056 | 0.1578 | 26.1 |
| Chi-Chi, Taiwan | 20-Sep-99 | TCU054 | SN | 7.6 | 5.3 | 6.6866 | 0.1689 | 61.2 |
| Parkfield, CA, USA | 28-Sep-04 | Parkfield Cholame 4A | SN | 6 | 4.69 | 0.8571 | 0.1856 | 22.16 |
| Chi-Chi, Taiwan | 20-Sep-99 | TCU128 | SN | 7.6 | 13.15 | 4.712 | 0.1874 | 78.3 |
| Chi-Chi, Taiwan | 20-Sep-99 | TCU042 | SN | 7.6 | 26.32 | 7.2152 | 0.2089 | 47.5 |
| Landers, CA, USA | 28-Jun-92 | Yermo Fire | SN | 7.28 | 23.62 | 6.841 | 0.2218 | 53.2 |
| Chi-Chi, Taiwan | 20-Sep-99 | TCU053 | SN | 7.6 | 5.97 | 9.7819 | 0.2247 | 41.9 |
| Irpinia, Italy-01 | 23-Nov-80 | Sturno | SN | 6.9 | 6.78 | 2.5442 | 0.2313 | 41.5 |
| Whittier Infrrows, USA | 10-Oct-87 | DOW | SN | 5.99 | 14.95 | 0.7305 | 0.2341 | 30.4 |
| Morgan Hill, CA, USA | 24-Apr-84 | Gilroy Array # 6 | SN | 6.19 | 9.85 | 1.1532 | 0.2430 | 35.4 |
| Chi-Chi, Taiwan | 20-Sep-99 | TCU082 | SN | 7.6 | 5.18 | 6.8932 | 0.2477 | 56.4 |
| Whittier Infrrows, USA | 10-Oct-87 | LB Orange Eve | SN | 5.99 | 19.8 | 0.7086 | 0.2554 | 32.9 |
| Izmit, Tukey | 17-Aug-99 | GBZ | SN | 7.51 | 7.57 | 4.6057 | 0.2633 | 41.4 |
| Northridge, CA, U.S.A. | 17-Jan-94 | LA Wadsworth VA Hospital North | SN | 6.7 | 14.55 | 2.27 | 0.2735 | 32.4 |
| Chi-Chi, Taiwan | 20-Sep-99 | TCU049 | SN | 7.6 | 3.78 | 9.2746 | 0.2810 | 45.1 |
| Superstition Hills, CA, USA | 24-Nov-87 | ELC | SN | 6.54 | 18.2 | 1.96 | 0.2973 | 52 |
| Chi-Chi, Taiwan | 20-Sep-99 | TCU076 | SN | 7.6 | 2.76 | 3.3714 | 0.3004 | 63.7 |
| Imperial Valley, USA | 15-Oct-79 | Agrarias | SN | 6.53 | 0 | 1.8766 | 0.3115 | 54.4 |
| Morgan Hill, CA, USA | 24-Apr-84 | HAL | SN | 6.19 | 3.45 | 0.8314 | 0.3141 | 39.7 |
| Ölfus, South Iceland | 25-May-08 | Selfoss City Hall | SN | 6.3 | 3.33 | 0.77 | 0.3232 | 33 |
| Chi-Chi, Taiwan | 20-Sep-99 | TCU075 | SN | 7.6 | 0.91 | 4.4338 | 0.3331 | 88.3 |
| Parkfield, CA, USA | 28-Sep-04 | Parkfield Cholame 2 east | SN | 6 | 2.5 | 0.82 | 0.3365 | 23.66 |
| South Iceland | 17-Jun-00 | FlagbjarInfrholt | SN | 6.57 | 4.2 | 1.8204 | 0.3401 | 72.24 |
| Palm Springs, CA, USA | 08-Jul-86 | DSP | SN | 6.06 | 0.99 | 1.28 | 0.3427 | 29.7 |
| Imperial Valley, USA | 15-Oct-79 | Aeroporto Mexicalli | SN | 6.53 | 0 | 1.5995 | 0.3573 | 44.3 |
| Loma Prieta, CA, USA | 17-Oct-89 | STG | SN | 6.93 | 7.58 | 1.5516 | 0.3653 | 57.2 |
| Imperial Valley, USA | 15-Oct-79 | EC Meloland Overpass FF | SN | 6.53 | 0.07 | 2.8518 | 0.3780 | 115 |
| L'Aquila, Italy | 06-Apr-09 | AQK | SN | 6.3 | 0 | 1.5754 | 0.3799 | 46.7 |
| Parkfield, CA, USA | 28-Sep-04 | Parkfield fault zone 12 | SN | 6 | 0.94 | 1.0056 | 0.3821 | 57.5 |
| Loma Prieta, CA, USA | 17-Oct-89 | Gilroy Array #2 | SN | 6.93 | 10.38 | 1.46 | 0.4062 | 45.7 |
| Superstition Hills, USA | 24-Nov-87 | PTS | SN | 6.54 | 0.95 | 1.8624 | 0.4186 | 106.8 |
| Northridge, CA, USA | 17-Jan-94 | NWS | SN | 6.7 | 2.11 | 2.025 | 0.4257 | 87.75 |
| Parkfield, CA, USA | 28-Sep-04 | Parkfield Cholame 3 west | SN | 6 | 2.5 | 0.6822 | 0.4416 | 45 |
| Coyote lake, CA, USA | 08-Jun-79 | GA6 | SN | 5.74 | 0.42 | 0.8189 | 0.4519 | 51.5 |
| Parkfield, CA, USA | 28-Sep-04 | Parkfield Cholame 2 west | SN | 6 | 1.88 | 0.8703 | 0.4605 | 49.98 |
| Chi-Chi, Taiwan aftershock | 20-Sep-99 | CHY080 | SN | 6.2 | 21.34 | 1.1017 | 0.4659 | 70.31 |
| Ölfus, South Iceland | 25-May-08 | Hveragerdi retirement house | S.N. | 6.3 | 1.4 | 1.43 | 0.4673 | 54 |
| Parkfield, CA, USA | 28-Sep-04 | Parkfield Cholame 1 east | SN | 6 | 1.88 | 1.0606 | 0.4713 | 52.82 |
| Parkfield, CA, USA | 27-Jun-66 | CO2 | SN | 6.19 | 6.27 | 1.68 | 0.4759 | 75.1 |
| Erzincan, Turkey | 13-Mar-92 | ERZ | SN | 6.69 | 0 | 2.2355 | 0.4834 | 95.4 |
| Ölfus, South Iceland | 25-May-08 | EERC, basement | SN | 6.3 | 3.33 | 0.78 | 0.4849 | 41.12 |
| Parkfield, CA, USA | 28-Sep-04 | Parkfield fault zone 1 | SN | 6 | 0 | 1.1186 | 0.4977 | 64.15 |
| Northridge, CA, USA | 17-Jan-94 | JFA | SN | 6.7 | 0 | 2.6631 | 0.5164 | 67.42 |
| Northridge, CA, USA | 17-Jan-94 | JFA generator | SN | 6.7 | 0 | 2.6631 | 0.5165 | 67.4 |
| Chi-Chi, Taiwan aftershock | 20-Sep-99 | TCU076 | SN | 6.2 | 13.04 | 0.7141 | 0.5238 | 58.9 |

*(continued)*

**Table 2.** (continued)

| Earthquake | Date | Station | Comp | M | $R_{jb}$ (km) | T (sec) | PGA (g) | PGV (cm/s) |
|---|---|---|---|---|---|---|---|---|
| South Iceland | 21-Jun-00 | Thorsartun | SN | 6.49 | 3.6 | 1.4937 | 0.5473 | 65.77 |
| Northridge, CA, USA | 17-Jan-94 | LA Dam (LDW) | SN | 6.7 | 0 | 1.2926 | 0.5700 | 75.21 |
| Parkfield, CA, USA | 28-Sep-04 | Parkfield Cholame 4 west | SN | 6 | 3.44 | 0.5815 | 0.5728 | 38.37 |
| Northridge, CA, USA | 17-Jan-94 | SCG | SN | 6.7 | 0 | 2.71 | 0.5943 | 130.3 |
| Gazli, USSR | 17-Mar-76 | KAR | SN | 6.8 | 3.92 | 4.1 | 0.6080 | 65.32 |
| Kobe, Japan | 19-Jan-95 | Takarazuka | SN | 6.9 | 0 | 1.2163 | 0.6452 | 72.6 |
| Loma Prieta, CA, USA | 17-Oct-89 | LGP | SN | 6.93 | 0 | 1.57 | 0.6461 | 103.2 |
| Palm Springs, CA, USA | 08-Jul-86 | NPS | SN | 6.06 | 0 | 1.0934 | 0.6659 | 73.64 |
| South Iceland | 21-Jun-00 | Solheimar | SN | 6.49 | 4.1 | 1.4489 | 0.6954 | 98.87 |
| Landers, CA, USA | 28-Jun-92 | LUC | SN | 7.28 | 2.19 | 4.0778 | 0.7088 | 140 |
| Northridge, CA, U.S.A. | 17-Jan-94 | Sylmar Olive View Medical FF | S.N. | 6.7 | 1.74 | 2.4123 | 0.7326 | 122.7 |
| Chi-Chi, Taiwan | 20-Sep-99 | TCU065 | SN | 7.6 | 0.59 | 4.3009 | 0.8218 | 127.8 |
| Northridge, CA, USA | 17-Jan-94 | SCH | SN | 6.7 | 0 | 2.9177 | 0.8387 | 116.6 |
| South Iceland | 21-Jun-00 | Thorsarbru | SN | 6.49 | 2.8 | 1.5398 | 0.8427 | 79.71 |
| San Salvador | 10-Oct-86 | Geotech investigation center | SN | 5.8 | 2.14 | 0.6668 | 0.8446 | 62.3 |
| Tabas, Iran | 16-Sep-78 | TAB | SP | 7.11 | 1.79 | 4.712 | 0.8472 | 117.7 |
| Chi-Chi, Taiwan | 20-Sep-99 | TCU129 | SN | 7.6 | 1.84 | 5.69 | 0.9816 | 71.47 |
| San FerInfndo, USA | 09-Feb-71 | PCD | SN | 6.61 | 0 | 1.1532 | 1.4345 | 116.5 |

M, magnitude; $R_{jb}$, Joyner-Boore distance; T, predominant period; PGA, peak ground acceleration; g, acceleration of gravity; PGV, peak ground velocity.

$$[C_t] = \lambda_1[M_t] + \lambda_2[K_t] \tag{6}$$

where $\lambda_1$ and $\lambda_2$ are Rayleigh factors being evaluated based on two natural frequencies of the building. To find natural frequencies and mode shapes of n-DOFs system, free vibration analysis is performed as follows:

$$([K_t] - \omega_t^2[M_t])\{\phi\} = [0] \tag{7}$$

$$\left| [K_t] - \omega_t^2[M_t] \right| = [0], \ A_t\{\phi\} \neq [0] \tag{8}$$

where $\omega_t$ and $\phi$ are natural frequencies and mode shapes of the structural system, respectively. Thus, natural frequencies can be used to evaluate the factors $\lambda_1$ and $\lambda_2$ by considering a 2% damping ratio for 1st to 5th modes. The damping ratios for the rest of the modes can be calculated as follows:

$$\xi_n = \xi_1 \left( \omega_1 \omega_5 + \omega_n^2 \right) / \left( \omega_n \omega_1 + \omega_5^2 \right) \tag{9}$$

The following two equations describe the Newmark step-by-step integration method used to solve equation (1)

$$\{x_s\}_{\tau + \Delta\tau} = \{x_s\}_\tau + \Delta\tau \{\dot{x}_s\} + \Delta\tau^2 \left[ (0.5 - \beta)\{\ddot{x}_s\} + \beta\{\ddot{x}_s\}_{\tau + \Delta\tau} \right] \tag{10}$$

$$\left\{\dot{x}_s\right\}_{\tau + \Delta\tau} = \left\{\dot{x}_s\right\}_\tau + \Delta\tau \left[ (1 - \gamma)\{\ddot{x}_s\} + \gamma\{\ddot{x}_s\}_{\tau + \Delta\tau} \right] \tag{11}$$

In which $\beta$ and $\gamma$ are Newmark's factors, and if the average acceleration method is used, they are taken as 1/4 and 1/2, respectively; and $\Delta\tau$ is the time step between two-time instances $\tau$ and $\tau + \Delta\tau$. Substituting Equation (10) and (11) into Equation (1), the following equation can be derived:

$$\{\Delta F_G\} = [K_t]\{\Delta x_{t,eff}\} \tag{12}$$

where $\{\Delta F_G\}$ and $\{\Delta x_{t,eff}\}$ are the incremental forces and the incremental displacement, respectively. However, the incremental forces in the time-step analysis are evaluated as follows:

$$\{\Delta F_G\} = -[M_t]\{r\}\Delta\ddot{x}_g + \left[\left(\frac{\gamma}{2\beta} - 1\right)\Delta\tau[C_t] + \frac{1}{2\beta}[M_t]\right]\{\ddot{x}_t\} + \left[\frac{\gamma}{\beta}[C_t] + \frac{1}{\beta\Delta\tau}[M_t]\right]\{\dot{x}_t\} + \{F_{err}\} \qquad (13)$$

The stiffness matrix of the benchmark building can be determined as follows:

$$[K_t] = \frac{1}{\beta(\Delta\tau)^2}[M_t] + \frac{\gamma}{\beta\Delta\tau}[C_t] + [K_D] \qquad (14)$$

Instead $[\boldsymbol{M_t}]$ and $[\boldsymbol{C_t}]$ are respectively the mass and damping matrices of the benchmark building, and $[\boldsymbol{K_D}]$ is the tangent stiffness matrix. The damping $[\boldsymbol{C_t}]$ matrix is as follows:

$$[C_t] = [T_R]^T[C_t][T_R] \qquad (15)$$

## Numerical study

Many researchers used the previously described 20-story benchmark building presented by Ohtori et al.[27] to investigate the effectiveness of different controller techniques. Some of them considered linear analysis, and others incorporated the structure's non-linear behavior by providing reasonable justifications for their assumptions and analysis procedures. In this work, for the first time, the effectiveness of an active controller for seismic response control of the benchmark building is investigated by comparing linear and non-linear analysis. In this first comparison, four earthquakes given in the package of the benchmark structure are initially used. Additionally, it is interesting to investigate whether the active control system is effective when the building is subjected to pulse-type ground motions. To this aim, a set of additional 69 pulse-type ground motions (see Table 2) is selected for this numerical study.

### Effectiveness of active controller

In this section, the active controller controls the benchmark building, as shown in Figure 1. Four natural ground motions, namely Imperial Valley, 1940; Hachinohe, 1968; Northridge, 1994; and Kobe, 1995, are selected to compare the performance of the active controller for seismic response mitigation of the building. Two different modelling assumptions are made and compared regarding the material behavior: in the first model, the building is assumed as linear elastic, whereas in the second model, the non-linear behavior of the building is incorporated into the analysis. Twenty-five control devices and five sensors are placed in the benchmark building, as shown in Figure 1. It is assumed that the system requires 20 computer resources to store or act for the process of response mitigation. Figure 3 shows the inter-story drift ratio of the uncontrolled (NC) building (top) and controlled building (bottom) while considering the linear and non-linear modelling.

The earthquake ground motions' peak ground acceleration (PGA) is 0.348 $g$; 0.229 $g$; 0.842 $g$; and 0.833 $g$, respectively, for Imperial Valley, 1940; Hachinohe, 1968; Northridge, 1994; and Kobe, 1995, where $g$ is the acceleration of gravity. It is noted that the incorporation of material non-linearity did not affect the response of both uncontrolled and controlled structures while subjected to earthquakes with low PGA. This implies that yielding phenomena are not triggered under such low-intensity ground motions, and therefore, the results of the two models coincide. However, in the case of ground motions with high PGA, the linear model has higher inter-story drift than expected. Engineers often use this condition to justify the usage of linear analysis. However, this is not very realistic in the case of a controlled building. Because of the lower difference between the two sets of results, a linear method might be adopted by researchers. By inspection of the acceleration response (see Figure 4), the differences between the two models tend to be even lower. However, to check this conclusion more carefully, a large set of pulse-like ground motions is selected and presented in the next section.

### Controlled and uncontrolled buildings under pulse-type ground motions

In this section, to clearly present the effectiveness of the active controller, a set of performance criteria are considered. The first three performance criteria (see Equations 16–18) denoted as $J_1, J_2$ and $J_3$ are the normalized peak inter-story drift, peak level acceleration, and base shear force, respectively.

$$J_1 = max\left\{\frac{\delta_C^{max}}{\delta_{NC}^{max}},\right\}, \ \delta_C^{max} = max_n\frac{|d_{C,n}(t)|}{h_n}, \ \delta_{NC}^{max} = max_n\frac{|d_{NC,n}(t)|}{h_n} \qquad (16)$$
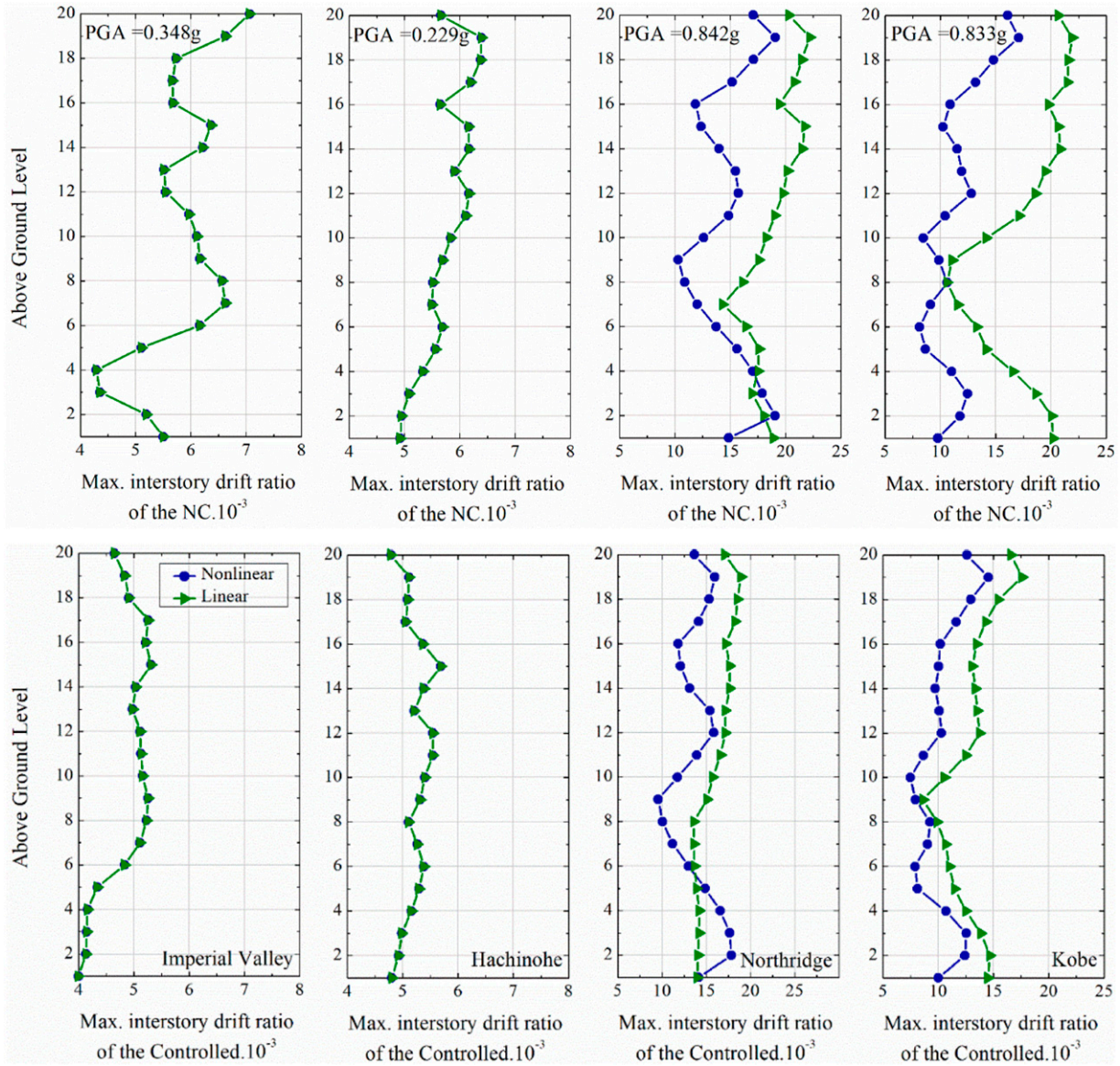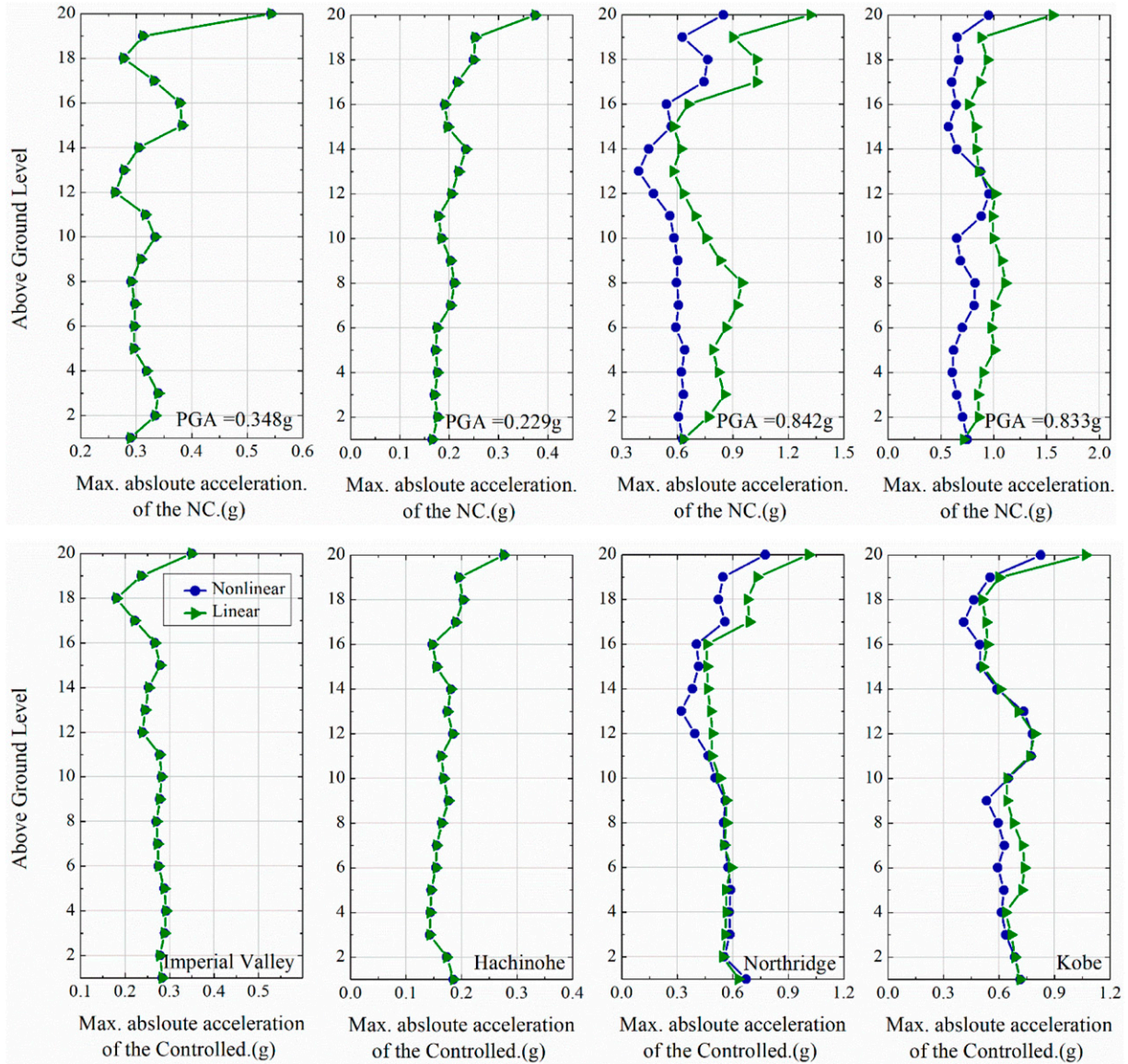
**Figure 3.** Peak inter-story drift ratio of the non-linear and linear modelling of the parent structure: uncontrolled (NC) building (top) and controlled building (bottom).

$$J_2 = max\left\{\frac{\ddot{X}_C^{max}}{\ddot{X}_{NC}^{max}},\right\}, \ddot{X}_C^{max} = \underset{n}{max}\left|\ddot{x}_{C,n}(t)\right|, \ddot{X}_{NC}^{max} = \underset{n}{max}\left|\ddot{x}_{NC,n}(t)\right| \tag{17}$$

$$J_3 = max\left\{\frac{F_{b,C}^{max}}{F_{b,NC}^{max}}\right\}, F_{b,C}^{max} = \underset{n}{max}\left|\sum_{n} m_n\ddot{x}_{C,n}(t)\right|, F_{b,NC}^{max} = \underset{n}{max}\left|\sum_{n} m_n\ddot{x}_{NC,n}(t)\right| \tag{18}$$

where $\delta^{max}$ is the maximum inter-story drift ratio; $d_n(t)$ is the inter-story drift at each level $n$ relative to the time history of 69 pulse-like ground motions; and $h_n$ is the height of the corresponding floors of the structure. Furthermore, the subscript $n = [1, \dots, 20]$ refers to the number story of benchmark building; $\ddot{X}^{max}$ is the vector of absolute acceleration at each level $n$; $F_b^{max}$ maximum base-shear force subjected to various level of ground motions records. In all variables, the subscripts C and NC refer to the controlled and uncontrolled building, respectively.

**Figure 4.** Peak story acceleration of the non-linear and linear modeling of the parent structure: uncontrolled building (NC) (top) and controlled building (bottom).

Details of the building and placement of the controllers are shown in Figure 1. Figure 2 shows the Simulink model for analyzing the controlled and uncontrolled buildings under pulse-type ground motions. In this study, equations (16) to (36) are used to define the set of performance criteria to quantify the effectiveness of the controller synthetically.

In most of them, a value lower than one indicates effectiveness in structural control (as the corresponding definition is normalized). As an example, Figure 5 reports the effectiveness in terms of peak inter-story drift ratio by considering four different variables, including characteristics of the structure and of the seismic excitation, namely the maximum inter-story drift ratio of uncontrolled (NC) building, the normalized fundamental period of the building divided by the dominant period of the earthquake ($\tau$) The peak ground acceleration (PGA) and the peak ground velocity (PGV). In this Figure 5, the results from non-linear analysis (Figure 5a) are compared to those obtained from linear analysis (Figure 5b). The earthquake ground motions are divided into three ranges based on their moment magnitude ($M_w$).

As reasonably expected, and as already noted for the previously considered four records, results for ground motions with low magnitude are not affected by the analysis type (linear vs non-linear) because the building is not yet yielded (minor damage or no damage at all occurred).
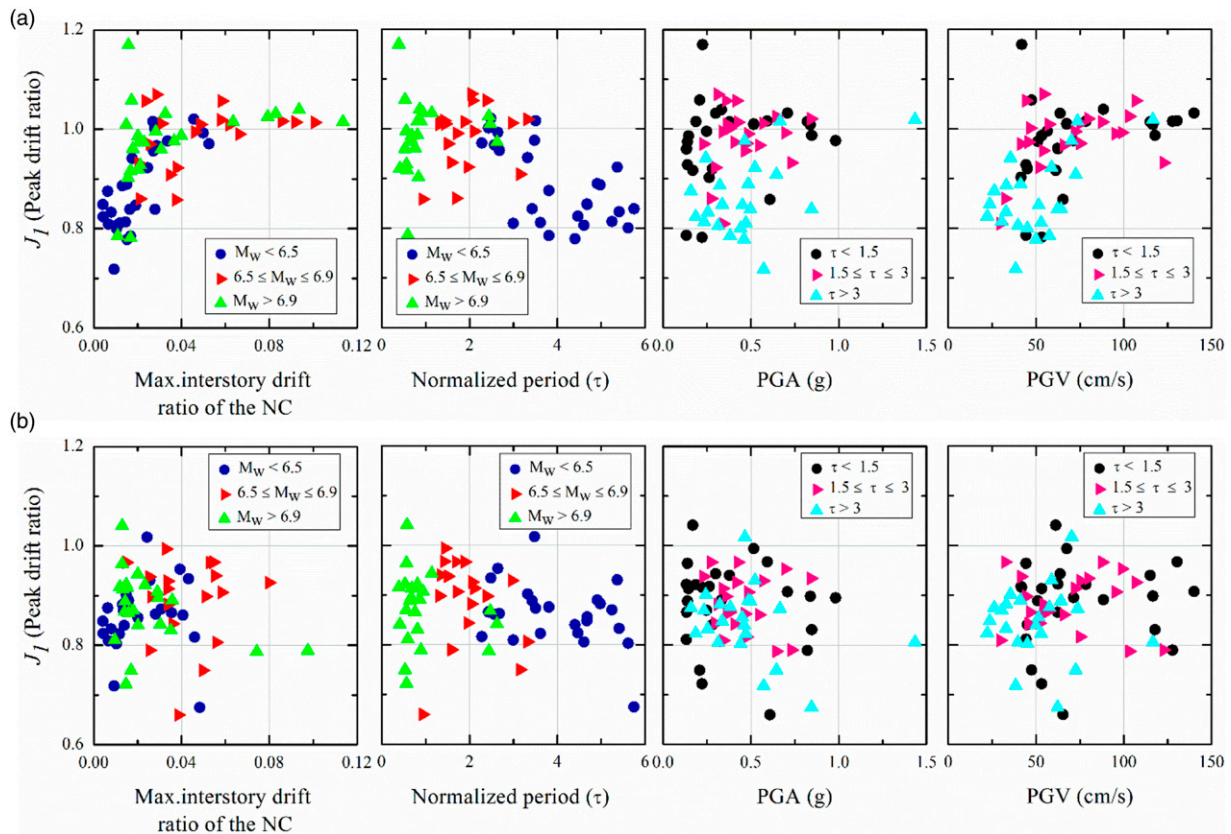
**Figure 5.** Peak inter-story drift ratio with respect to multiple parameters for (a) non-linear and (b) linear modelling of the parent structure.

However, the linear analysis cannot be considered for the increasing magnitude of the ground motions. Indeed, it is found that the structure will undergo damage in this situation, and the controller is less effective.

Therefore, linear analysis is not recommended for the building with active control subjected to severe pulse-type earthquake excitations. It is also worth noticing that high magnitude ground motions also fall in the range of resonance (or quasi-resonance) condition with the structure ($\tau \approx 1$) this justifies why the structure is more damaged under such a resonant condition. Also, PGA and PGV values confirm the fact that considering the linear analysis can mislead the assessment of the controller performance. Indeed, the controller performs well in reducing the seismic response, but in reality, the structure is already collapsed (which cannot be accounted for with a linear material model).

Figure 6 shows the peak story acceleration and is an important criterion for checking secondary structures' safety and acceleration-sensitive equipment during earthquakes. It is seen that the response of uncontrolled building has a significantly higher acceleration response in the case of linear analysis as compared to non-linear analysis. Moreover, the response reduction is quite high by applying the active controller. In a realistic condition, the building gets damaged during the earthquake, which increases the structural period; therefore, the acceleration response obtained from the non-linear analysis is lower than that calculated from the linear analysis. But the active controller seems to be less effective while non-linear analysis is considered.

Figure 7 displays the peak base shear of the building under the pulse-type ground motions. As seen above for the acceleration response, similar conclusions can be drawn that the response is significantly lower while the non-linear model is considered. At the same time, the controller is less effective in reducing the damaged building response, even though the response is amplified in some cases. This could be more clearly seen by analyzing the trend of the results in terms of PGV, which is a better indicator for displaying the resonance condition and for synthetizing the severity level of the pulse-type ground motions.

A better response reduction is observed in the linear structure, which may be misleading since the linearity of a structure cannot be guaranteed under strong pulse-like ground motions.
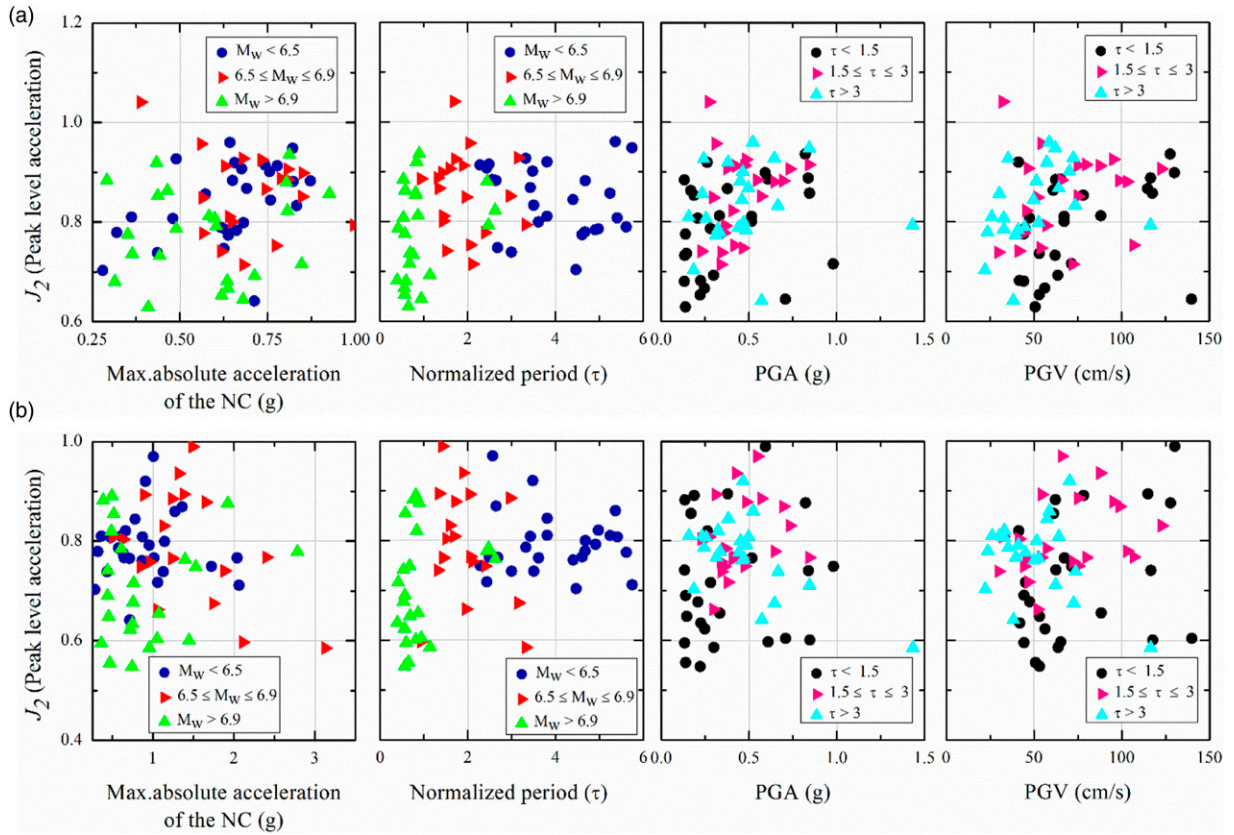
**Figure 6.** Peak story acceleration with respect to multiple parameters for (a) non-linear and (b) linear modelling of the parent structure.
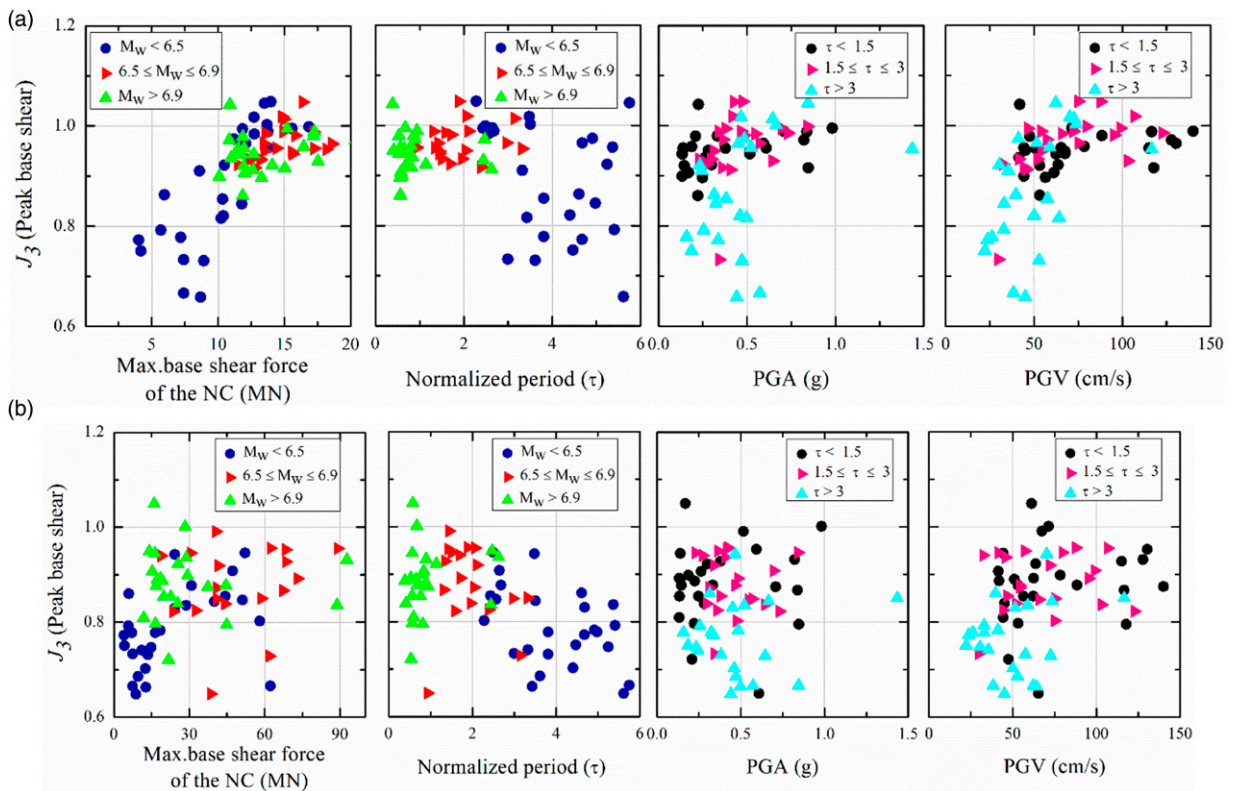


**Figure 7.** Peak base shear with respect to multiple parameters for (a) non-linear and (b) linear modelling of the parent structure.

The next three performance criteria (see equations (19)–(21)) $J_4, J_5$ and $J_6$, depicts the norm, ($\|.\| = \sqrt{\frac{1}{t_f} \int_0^{t_f} [.]^2 dt}$) response of the building. Where $t_f$ and $dt$, respectively, are the duration and time step of the ground motions.

$$J_4 = max\left\{\frac{\left\|\delta_C^{max}\right\|}{\left\|\delta_{NC}^{max}\right\|}\right\} \tag{19}$$

$$J_5 = max\left\{\frac{\left\|\ddot{X}_C^{max}\right\|}{\left\|\ddot{X}_{NC}^{max}\right\|}\right\} \tag{20}$$

$$J_6 = max\left\{\frac{\left\|F_{b,C}^{max}\right\|}{\left\|F_{b,NC}^{max}\right\|}\right\} \tag{21}$$

Figure 8 shows the norm of inter-story drift ratio for linear and non-linear structure controlled by an active controller while subjected to pulse-like ground motions. Norm response is a useful and synthetic indicator representative of the entire response, as it covers multiple peaks during the time history. This is especially important because the structure may get damaged during the main peak occurrence and due to accumulation of damage over the entire time history. In these cases, similar to previous cases, linear analysis is misleading as it predicts that the controller is very effective. However, for non-linear analysis the seismic response is increased up to 20%. Similarly, Figure 9 shows the norm of story acceleration in both non-linear and linear models of the buildings under pulse-like ground motions. Similar reduction patterns can be observed in considering both the non-linear and the linear approach (only in weak ground motions). A similar pattern can be seen for norm base shear (see Figure 10). The other performance criteria (see equations (22) to (25)) are named as $J_7, J_8$ and $J_9, J_{10}$. They allow one to estimate the building damage by means of ductility, dissipated energy, plastic connections (hinges), and norm of ductility coefficient, respectively.
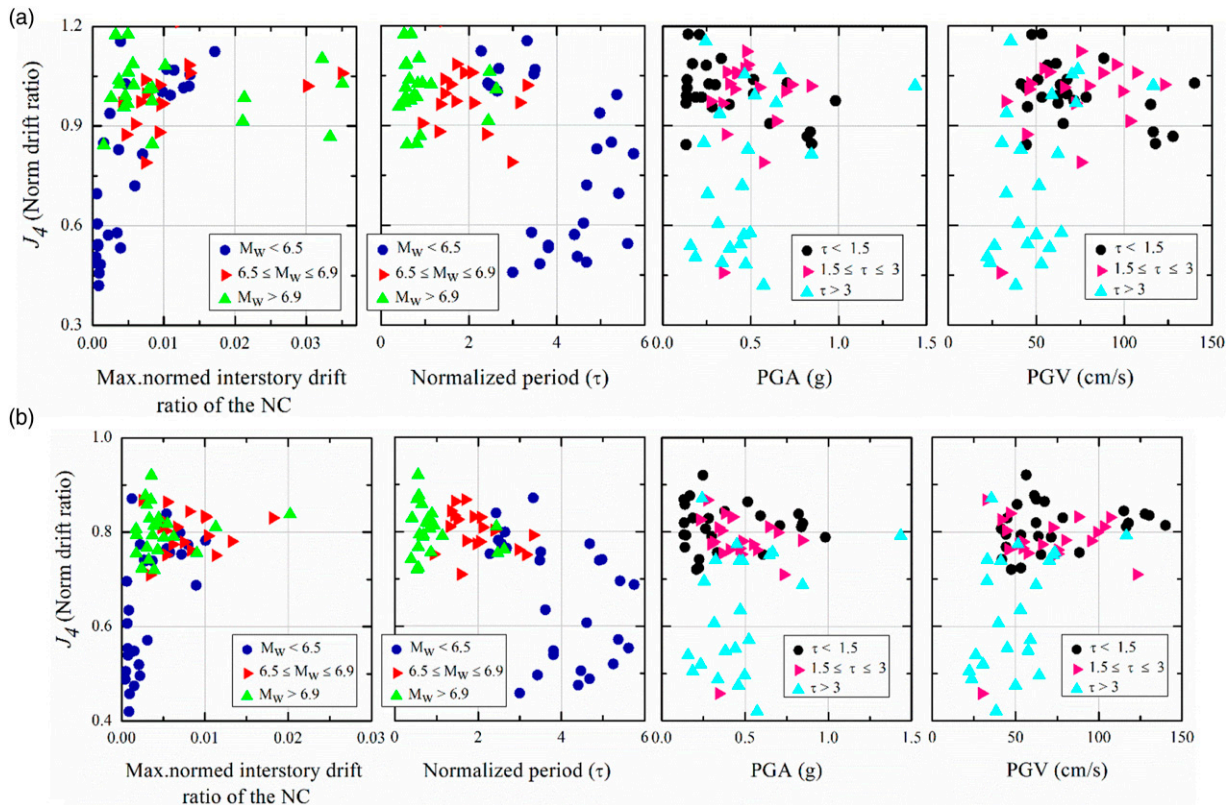


**Figure 8.** Norm drift ratio with respect to multiple parameters for (a) non-linear and (b) linear modelling of the parent structure.

$$J_7 = max\left\{\frac{\phi_C^{max}}{\phi_{NC}^{max}}\right\}, \phi_C^{max} = max\frac{|\phi_{C,j}(t)|}{\phi_{C,yj}}, \phi_{NC}^{max} = max\frac{|\phi_{NC,j}(t)|}{\phi_{NC,yj}} \tag{22}$$

$$J_8 = max\left\{\frac{E_C^{max}}{E_{NC}^{max}}\right\}, E_C^{max} = \frac{\int dE_{C,j}}{F_{C,yj}.\phi_{C,yj}}, E_{NC}^{max} = \frac{\int dE_{NC,j}}{F_{NC,yj}.\phi_{NC,yj}} \tag{23}$$

$$J_9 = max\left\{\frac{N_{C,d}}{N_{NC,d}}\right\} \tag{24}$$

$$J_{10} = max\left\{\frac{\|\phi_C^{max}\|}{\|\phi_{NC}^{max}\|}\right\} \tag{25}$$

where, $\phi_j, \phi_{yj}$ and $F_{NC,yj}$ represent bending curvature, yield curvature, and yield moment at the end of the $j^{th}$ element (member), respectively; as well as $\phi^{max}$, $E^{max}$ and $\int dE_j$ represents maximum curvature, maximum dissipated energy (maximum of all element ends and over time), and dissipated energy at the ends of the member, respectively, relative to the ground motion. Furthermore, $N_d$ represents the number of damaged connections (member ends). Figure 11 shows the variation of ductility of the building, dissipated energy in yielded joints, number of plastic connections, and norm ductility of the building under the considered ground motions. It is observed that strong earthquakes cause large curvatures that affect the structure's ductility inversely. In low magnitude earthquakes, the controller is quite effective because the structure is not yielded or has undergone minor damage. It is seen that PGA is not a clear intensity measure for damage assessment of structures subjected to pulse-like ground motions as the trend results are quite dispersed. On the contrary, the PGV could be
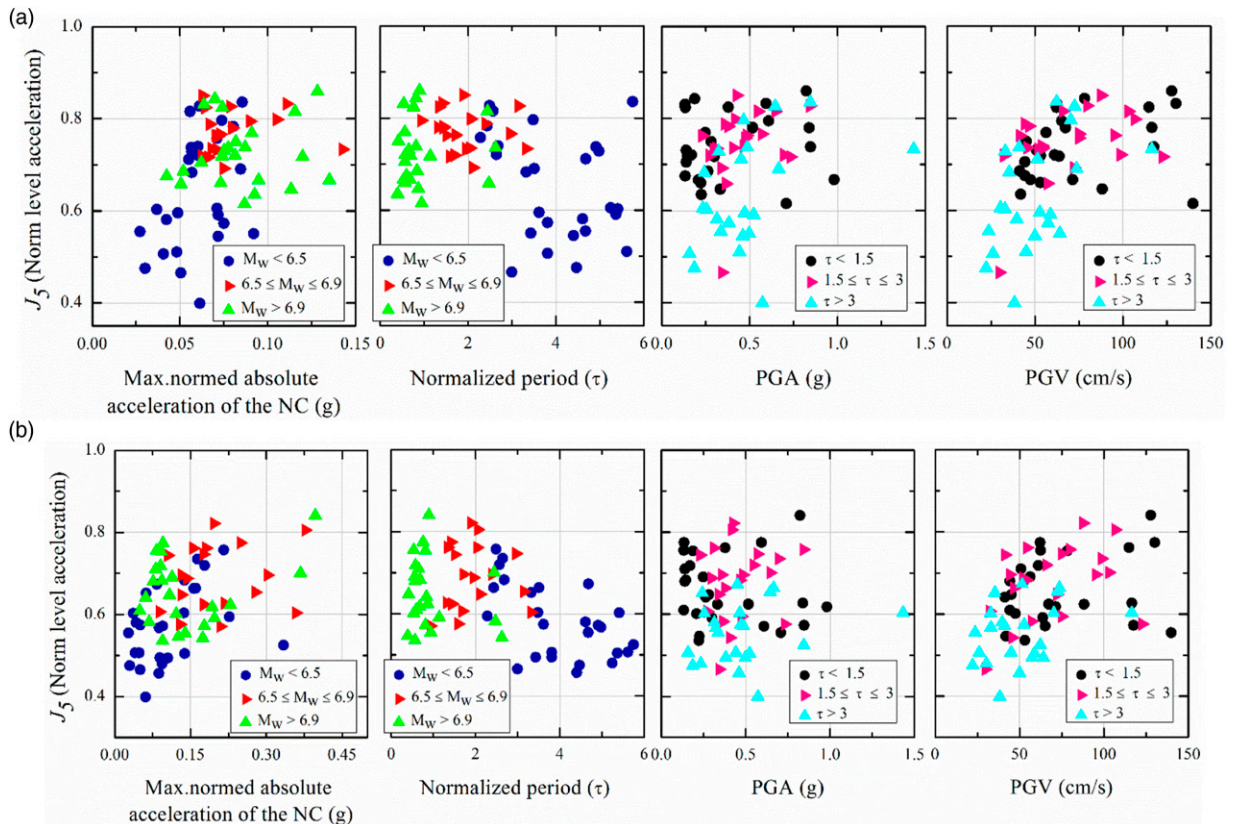


**Figure 9.** Norm level acceleration with respect to multiple parameters for (a) non-linear and (b) linear modelling of the parent structure.
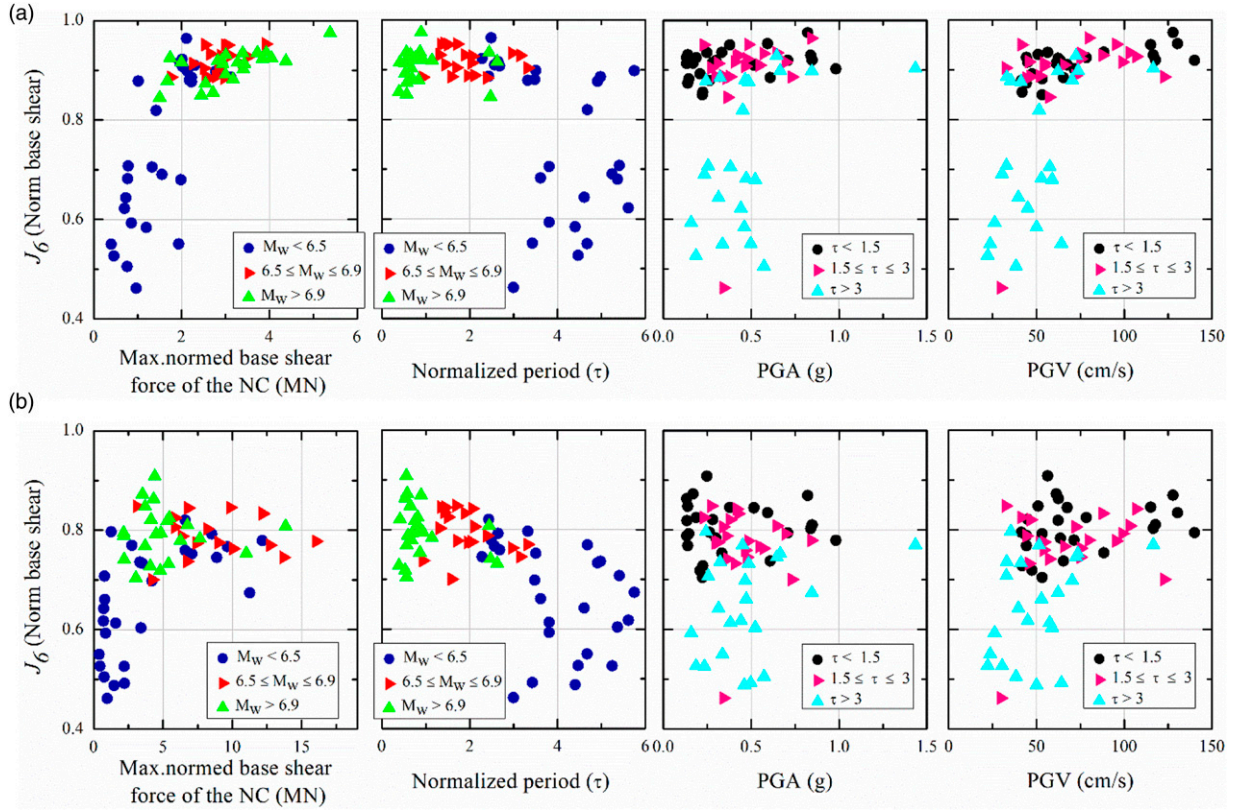
**Figure 10.** Norm base shear with respect to multiple parameters for (a) non-linear and (b) linear modelling of the parent structure.

a better option to be the intensity measure because the pattern of the responses is more evident when considering the PGV as an intensity measure.

The following four performance criteria (see equations (26) to (29)) $J_{11}, J_{12}$ and $J_{13}, J_{14}$ govern the control device's state, control force, control device stroke, and power needed for control, involving a measure of the total power expected for the control of the structure.

$$J_{11} = max\left\{\frac{\underset{\tau,l}{max}|f_l(\tau)|}{W}\right\}, W = \left[\sum_{i=1}^{i=n} m_i\right]g, g = 9.81\left(m/s^2\right) \tag{26}$$

$$J_{12} = max\left\{\frac{\underset{\tau,l}{max}|y_l^a(\tau)|}{x_{NC}^{max}}\right\} \tag{27}$$

$$J_{13} = max\left\{\frac{\underset{\tau,l}{max}\left[\sum_l P_l(\tau)\right]}{x_{NC}^{max}W}\right\}, P_l(\tau) = \left|\dot{y}_l^a(\tau)f_l(\tau)\right| \tag{28}$$

$$J_{14} = max\left\{\frac{\sum_l \frac{1}{t_f}\int_0^{t_f} P_l(t)}{\dot{x}^{max}}\right\} \tag{29}$$
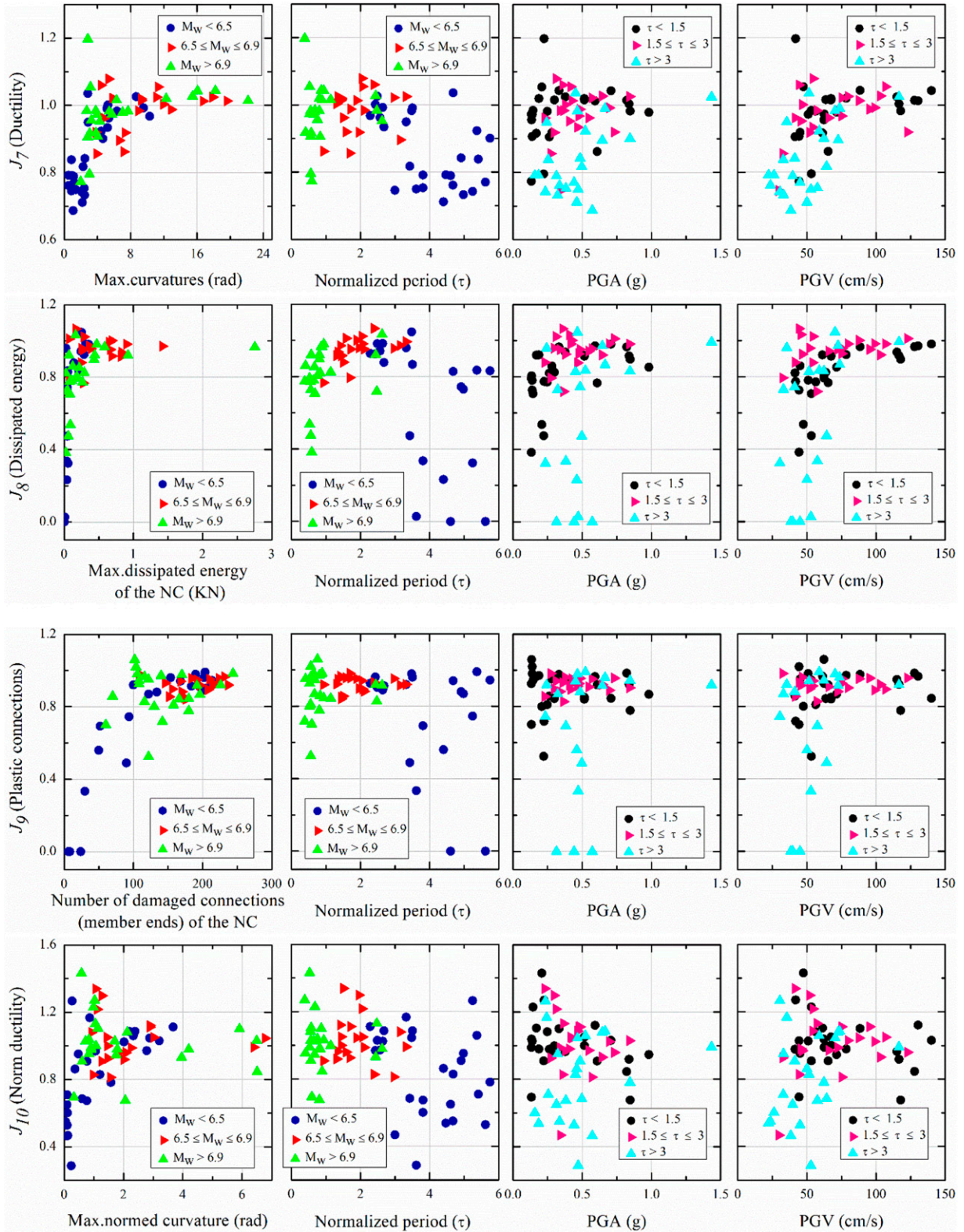
**Figure 11.** Ductility, dissipated energy, and plastic connections (hinges), normed of ductility coefficient with respect to multiple parameters for non-linear modelling of the parent structure.

where $f_l(\tau)$ is the force generated by the control device relative to each ground motion (time history). The subscript $l = [1, ..., 25]$ refers to the number of the semi-active device incorporated in the benchmark building; $W$ is the total weight of the building by neglecting the mass of floors below the ground. $y_l^a(\tau)$ and $\dot{y}_l^a(\tau)$ are displacement (stroke) and velocity of semi-active control devices during the ground motions, whereas $x_{NC}^{max}$ and $\dot{x}_{NC}^{max}$ are the maximum uncontrolled displacement and velocity at each floor level of benchmark building. $P_l(\tau)$ is the actual power required by the semi-active device to properly operate. Further, regardless of passive control, state devices $J_{14}$ take zeros. Figure 12 shows the control forces required for the devices to reduce the response effectively. In linear modelling, the PGA and PGV are the main intensity to decide the amount of control force required, whereas, in the case of non-linear model, a clear pattern is not observed. Therefore, there is scope to establish an optimization technique to obtain the optimum parameters of the devices for controlling the response of non-linear models.

Also, the stroke of the device shows that in the non-linear model, the devices are not effectively mitigating the response because they exhibit reduced stroke compared to the linear model (see Figure 13). This indicates that due to significant changes in the frequency of the building occurring in the more realistic non-linear model, the controller cannot effectively reduce the response. Also, the linear analysis is misleading to estimate the required control power (Figures 14 and 15). This is a critical result while designing an active or semi-active system. Therefore, adopting linear analysis for such conditions is totally not recommended.

The other performance criteria (see equations (30)–(32)) $J_{15}, J_{16}$ and $J_{17}$ aim to elaborate on the benefits and capabilities of the control strategy of each method.

They defined the total number of control devices realized to control the benchmark building, the total number of control sensors employed for the control strategy and $J_{17}$ is a criterion related to the computational resources needed, which is represented by the dimension of the discrete state vector $x_k^c$ necessary for the control algorithm. It is worth mentioning that in this study, 25 control devices ($J_{15} = 15$), five sensors ($J_{16} = 5$), and 20 computer resources ($J_{17} = 20$) are used.

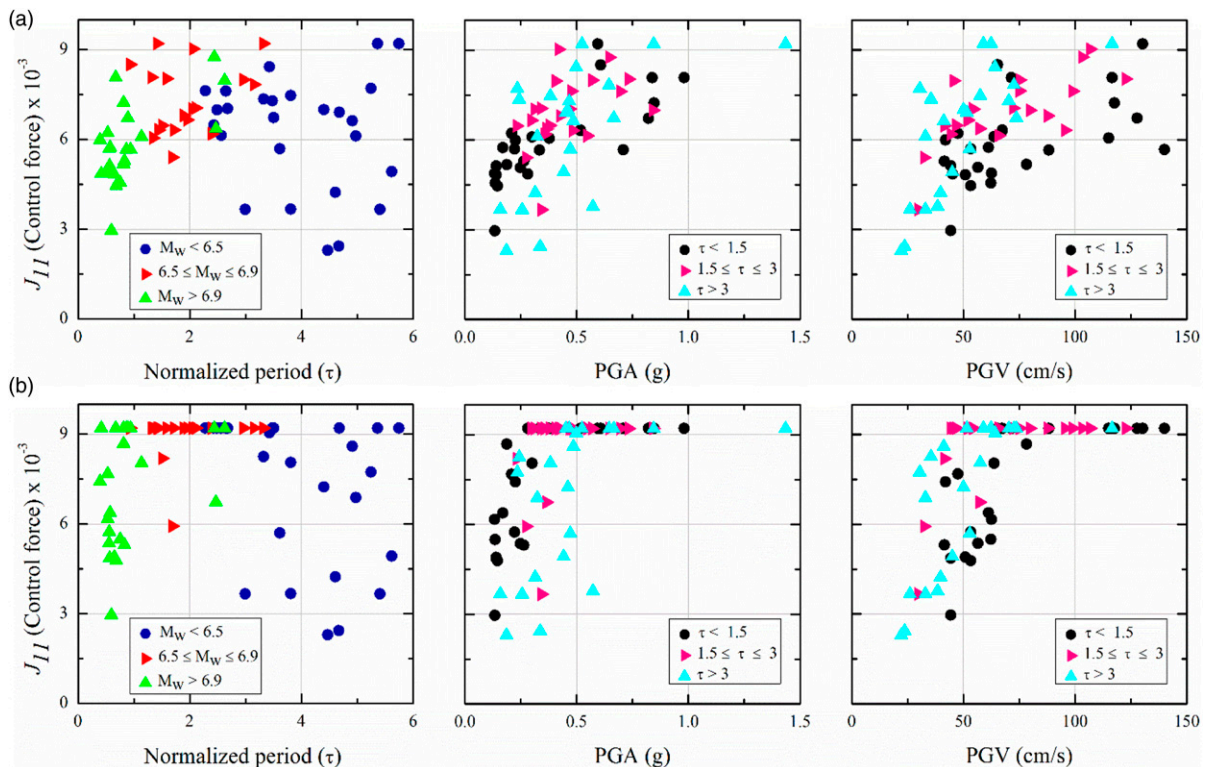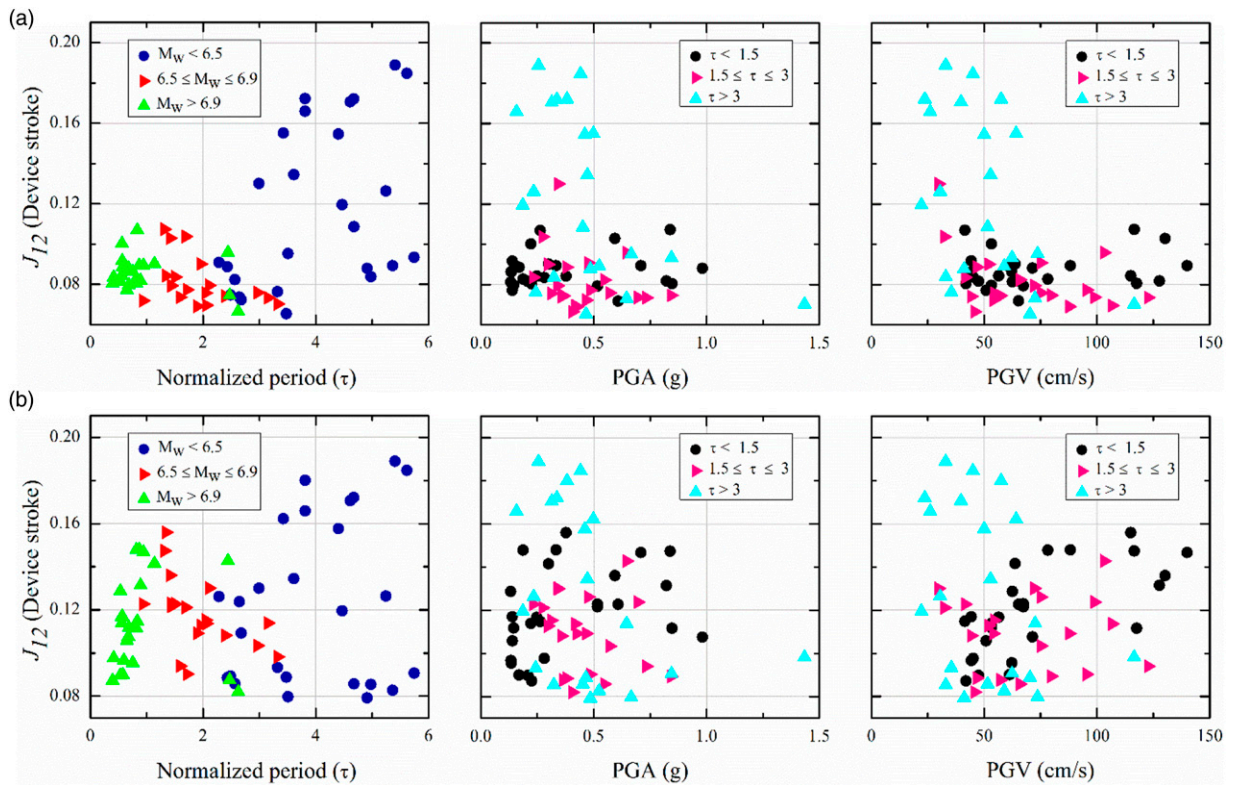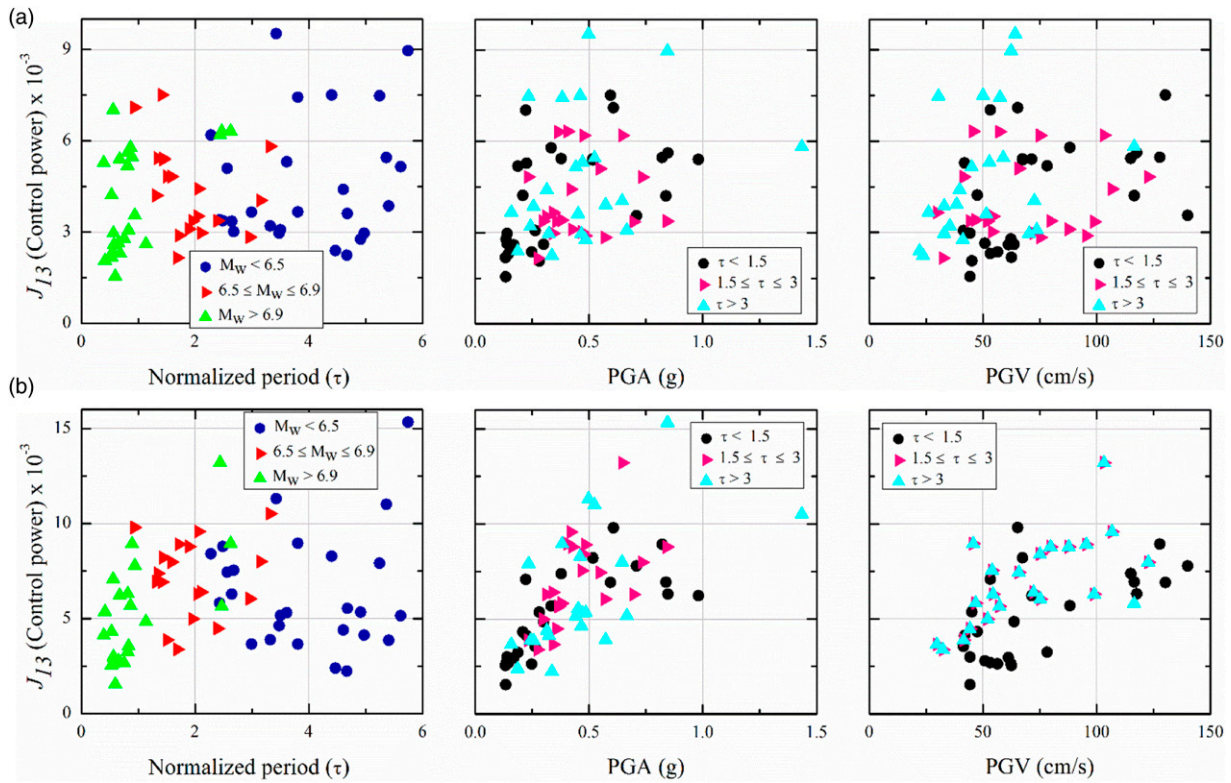$$J_{15} = \text{Number of control devices} \tag{30}$$



**Figure 12.** Control force with respect to multiple parameters for non-linear modelling of the parent structure. (a) Non-linear structure. (b) Linear structure.

$$J_{16} = \text{Number of required sensors} \tag{31}$$

$$J_{17} = dim(x_k^c) \tag{32}$$

In a similar manner, $J_{18}, J_{19}, J_{20}$ and $J_{21}$ are performance criteria (see equations (33) to (36)) indicating the maximum absolute displacement, maximum absolute velocity, norm of maximum displacement, and norm of maximum velocity, respectively, of controlled and uncontrolled building.

$$J_{18} = max\left\{\frac{x_C^{max}}{x_{NC}^{max}}\right\} \tag{33}$$

$$J_{19} = max\left\{\frac{\dot{x}_C^{max}}{\dot{x}_{NC}^{max}}\right\} \tag{34}$$

$$J_{20} = max\left\{\frac{\left\|x_C^{max}\right\|}{\left\|x_{NC}^{max}\right\|}\right\} \tag{35}$$

$$J_{21} = max\left\{\frac{\left\|\dot{x}_C^{max}\right\|}{\left\|\dot{x}_{NC}^{max}\right\|}\right\} \tag{36}$$



**Figure 13.** Stroke of the device with respect to multiple parameters for non-linear modelling of the parent structure. (a) Non-linear structure. (b) Linear structure.

**Figure 14.** Control power with respect to multiple parameters for non-linear modelling of the parent structure. (a) Non-linear structure. (b) Linear structure.
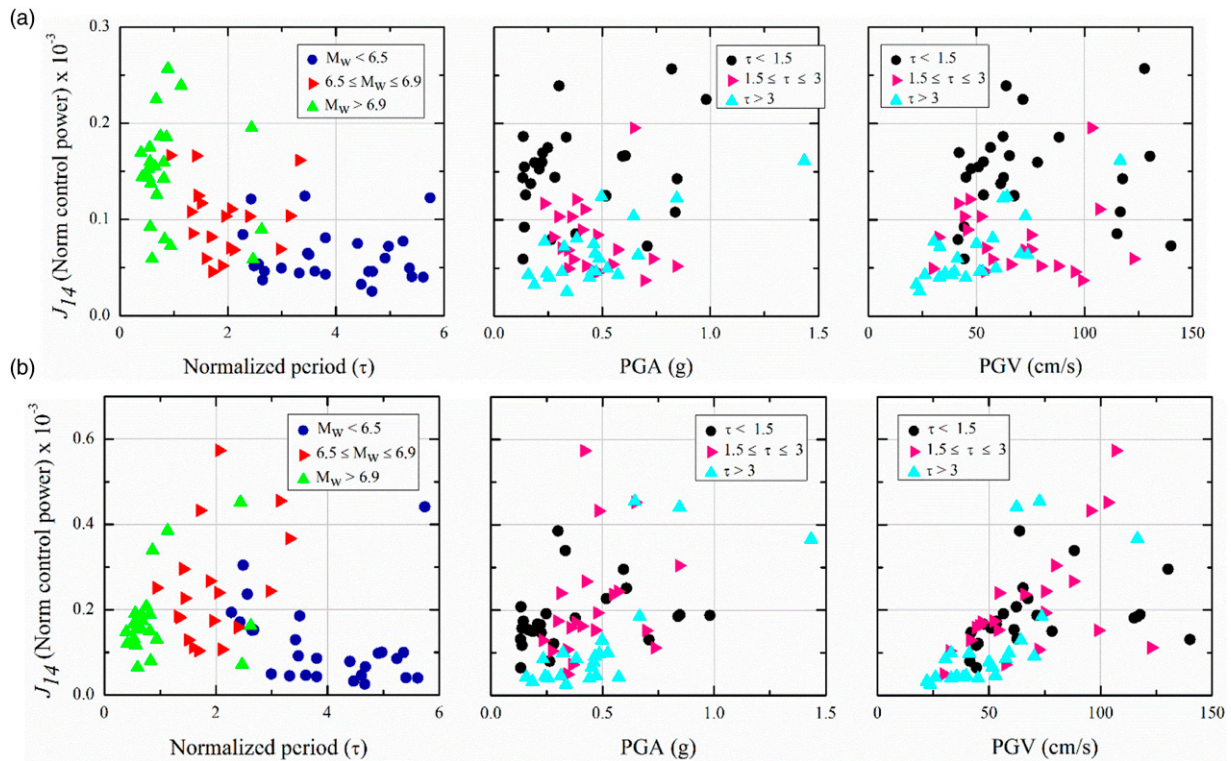


**Figure 15.** Norm of control power with respect to multiple parameters for non-linear modelling of the parent structure. (a) Non-linear structure. (b) Linear structure.
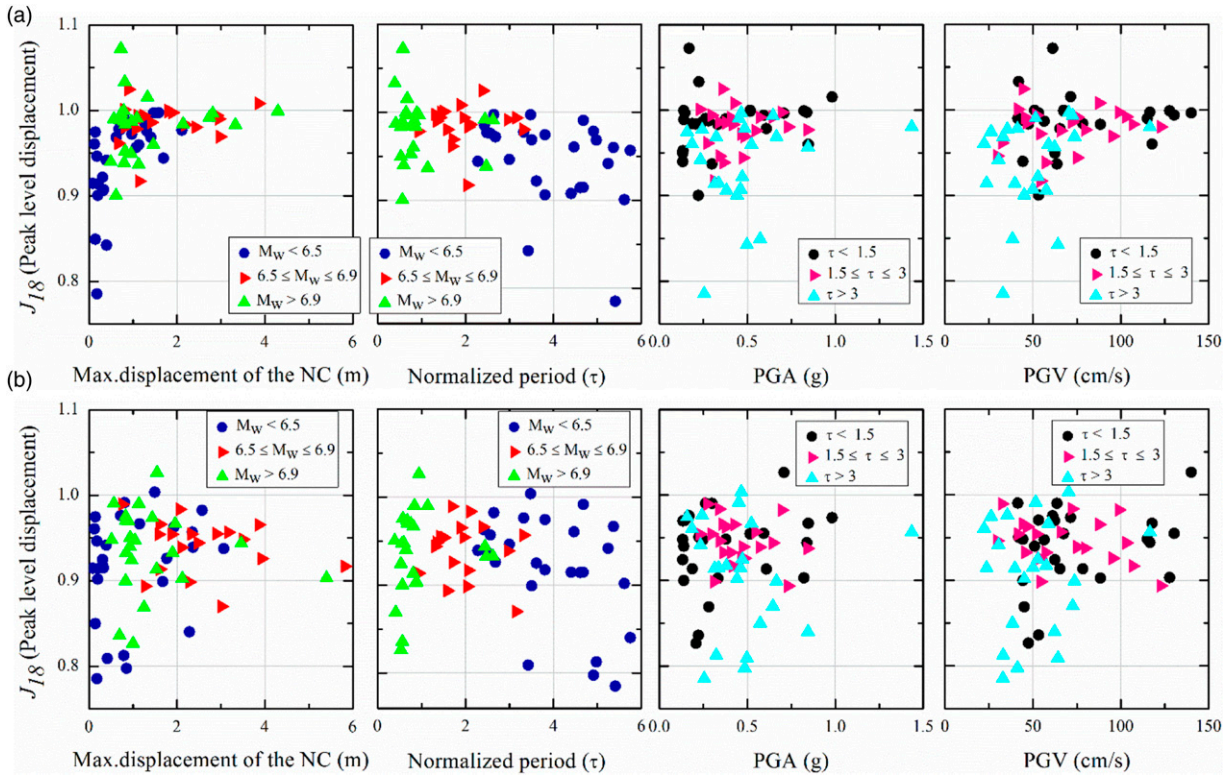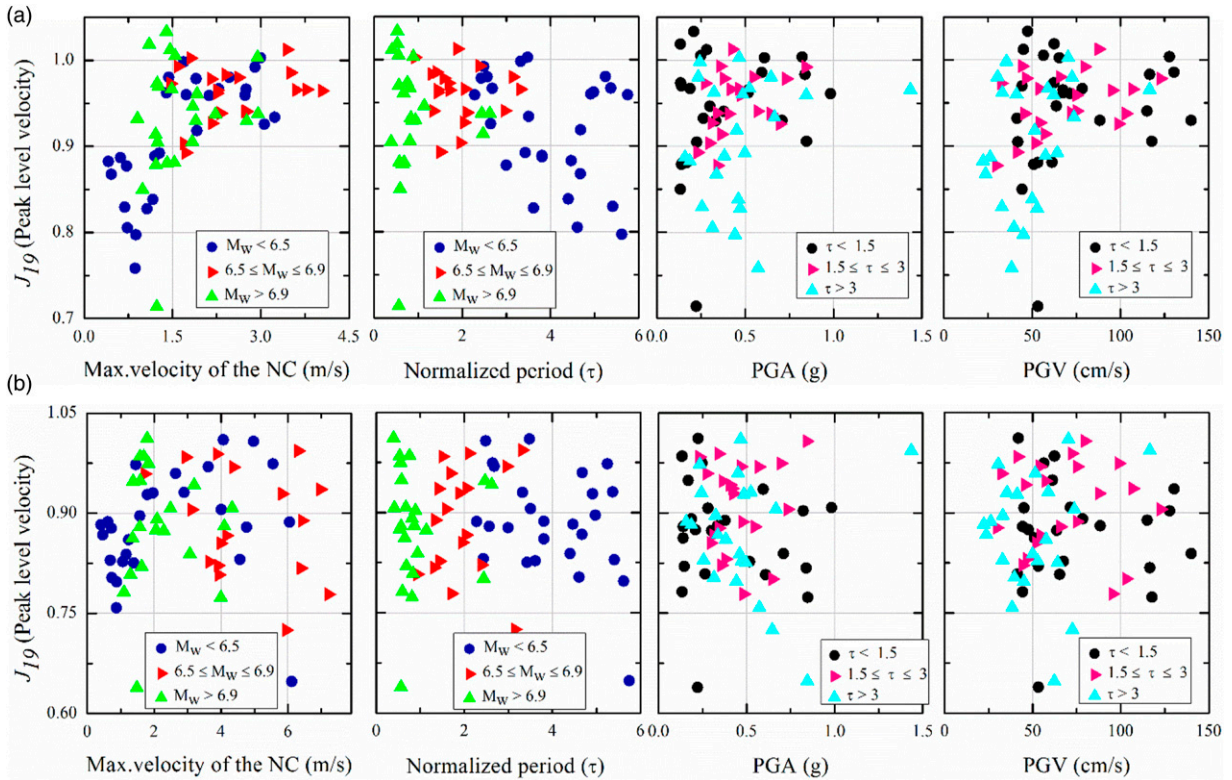
**Figure 16.** Peak displacement response with respect to multiple parameters for non-linear modelling of the parent structure. (a) Non-linear structure. (b) Linear structure.



**Figure 17.** Peak velocity response with respect to multiple parameters for non-linear modelling of the parent structure. (a) Non-linear structure. (b) Linear structure.
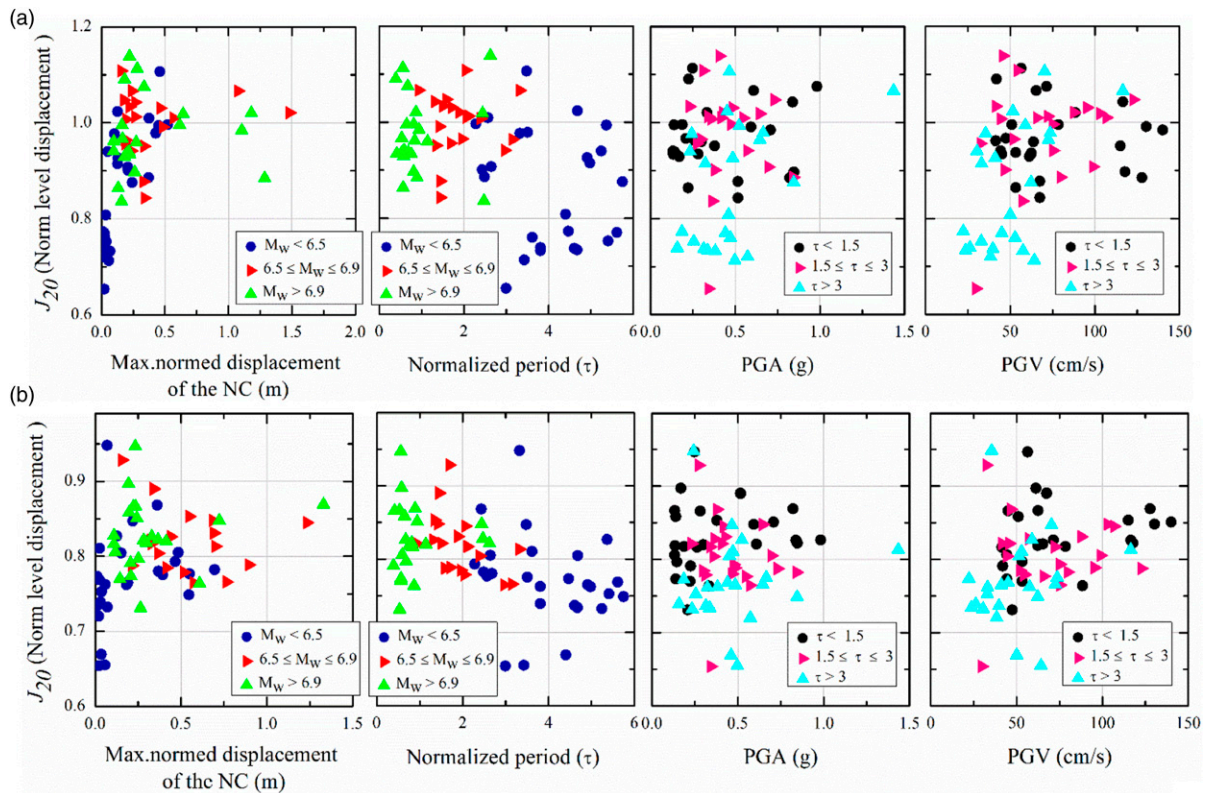
**Figure 18.** Norm of displacement response with respect to multiple parameters for non-linear modelling of the parent structure. (a) Non-linear structure. (b) Linear structure.
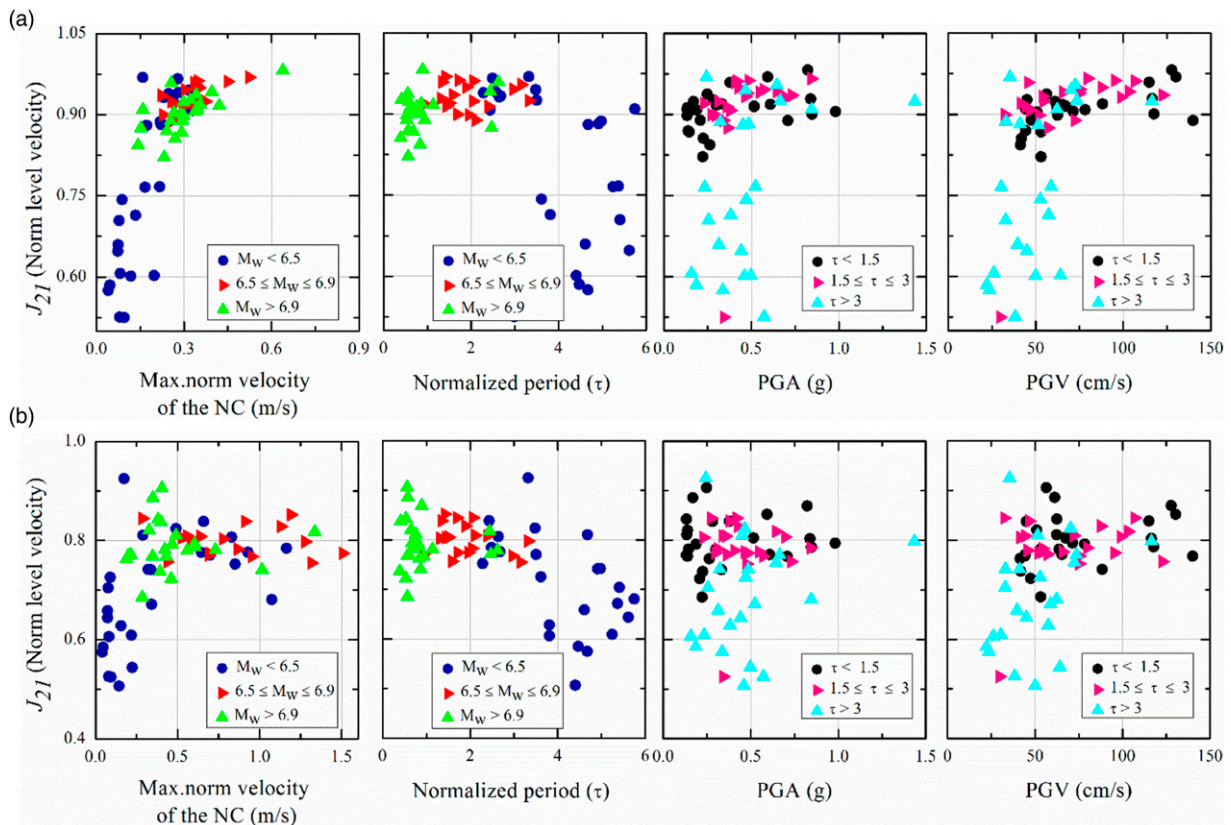


**Figure 19.** Norm of velocity response with respect to multiple parameters for non-linear modelling of the parent structure. (a) Non-linear structure. (b) Linear structure.

Figures 16 and 17 show the variation of the buildings' peak displacement and peak velocity under the pulse-like ground motions. It is again observed that the PGV is more accurate as an intensity measure for the assessment of the structure subjected to pulse-like ground motions than PGA. It is also observed that near the resonance condition, the controller is not effective in non-linear model, whereas it seems more effective in linear modelling. This again confirms that the analysis method has a significant influence on the outcomes of the seismic analysis under pulse-type ground motions.

A similar trend is observed while considering the displacement norm (see Figure 18) and norm of velocity (see Figure 19). Therefore, it is concluded that non-linear analysis should be considered to assess the robustness of the controllers for seismic response mitigation of buildings subjected to pulse-like ground motions. Also, the PGV is an accurate intensity measure for assessing structures subjected to pulse-like ground motions.

## Conclusions

The performance of the active controller for seismic response mitigation of a benchmark steel building under pulse-type ground motions has been presented. Peak ground acceleration (PGA) and peak ground velocity (PGV) are tested as potential intensity measures for the performance assessment of the buildings subjected to pulse-like ground motions. Two types of modelling assumptions are considered in this numerical study, namely, (i) non-linear modelling by considering that beam-column joints can yield and (ii) an indefinitely linear elastic model. Based on the results presented, the following conclusions are drawn:

1. The controller shows significantly high performance in reducing significant seismic response when considering a linear elastic building model. However, under such severe earthquake excitations, the structure is collapsed, and the controller is less effective if a more realistic non-linear analysis incorporating material non-linear behavior is performed. This misleads researchers and engineers in understanding the true performance of controllers if the linear analysis is adopted. Therefore, it is recommended to consider non-linear analysis for assessing the performance of the controllers.
2. The PGV is an accurate intensity measure for the assessment of the structures subjected to pulse-like ground motions.
3. Ground motions having a higher magnitude and a dominant period close to the structure period cause major damage; therefore, the linear model must not be applied in such conditions.
4. To improve the effectiveness of the controllers for response mitigation of non-linear models under pulse-like ground motions, a novel optimization technique is undoubtedly required.

Three studies that require special consideration in the future scope of the authors are (i) checking the effectiveness of passive, semi-active, and hybrid controllers for a realistic situation of non-linear modelling. Additionally, current optimization techniques require improvement if the parent structure is not elastic; (ii) Fragility analysis of structures subjected to pulse-like ground motions; and (iii) investigation of the performance of semi-active controller for non-linear benchmark building by optimizing both the number as well as the proper location of sensors and actuators required for best performance through multi-objective optimization. However, a novel meta-heuristic algorithm is performed for the analysis subjected to pulse-like ground motions.

## ORCID iDs

Said Elias ⊙ https://orcid.org/0000-0002-8231-9765
Mahdi Abdeddaim ⊙ https://orcid.org/0000-0001-5775-9403

## References

1. Elias S and Matsagar V. Research developments in vibration control of structures using passive tuned mass dampers. *Annu Rev Control* 2017; 44: 129–156.

2. Amjadian M. *Development of Electromagnetic Friction Dampers for Improving Seismic Performance of Civil Structures* (Doctoral dissertation, The City College of New York), 2019.

3. Amjadian M and Agrawal AK. Seismic response control of multi-story base-isolated buildings using a smart electromagnetic friction damper with smooth hysteretic behavior. *Mech Syst Signal Process* 2019; 130: 409–432.

4. Soto MG and Adeli H. Semi-active vibration control of smart isolated highway bridge structures using replicator dynamics. *Eng Struct* 2019; 186: 536–552.

5. Azar BF, Veladi H, Raeesi F, et al. Control of the nonlinear building using an optimum inverse TSK model of MR damper based on modified grey wolf optimizer. *Eng Structures* 2020; 214: 110657.

6. Raeesi F, Azar BF, Veladi H, et al. An inverse TSK model of MR damper for vibration control of nonlinear structures using an improved grasshopper optimization algorithm. *Structures* 2020; 26: 406–416.

7. Zhao J, Li K, Zhang XC, et al. Multidimensional vibration reduction control of the frame structure with magnetorheological damper. *Struct Control Health Monit* 2020; 27(8): e2572.

8. Lu Z, Masri SF, and Lu X. Optimization design of impact dampers and particle dampers. In *Particle Damping Technology Based Structural Control*. Singapore: Springer, 2020.

9. Lu Z, Masri SF, and Lu X. Semi-active control particle damping technology. In *Particle Damping Technology Based Structural Control*. Singapore: Springer, 2020.

10. Hormozabad SJ and Soto MG. Load balancing and neural dynamic model to optimize replicator dynamics controllers for vibration reduction of highway bridge structures. *Eng Appl Artif Intelligence* 2021; 99: 104138.

11. Saeed MU, Sun Z, and Elias S. Semi-active vibration control of building structure by self tuned brain emotional learning based intelligent controller. *J Building Eng* 2022; 46: 103664.

12. Yanik A. Absolute instantaneous optimal control performance index for active vibration control of structures under seismic excitation. *Shock and Vibration*, 2019; 2019: 1–13.

13. Yanik A, Aldemir U, and Bakioglu M. A new active control performance index for vibration control of three-dimensional structures. *Eng Structures* 2014; 62: 53–64.

14. Yanik A, Aldemir U, and Bakioglu M. Active control of three-dimensional structures. *Dyn Civil Structures* 2014; 4: 479–486.

15. Moghaddasie B and Jalaeefar A. Optimization of LQR method for the active control of seismically excited structures. *Smart Structures Syst* 2019; 23(3): 243–261.

16. Ümütlü RC, Ozturk H, and Bidikli B. A robust adaptive control design for active tuned mass damper systems of multistory buildings. *J Vibration Control* 2020; 27: 1077546320966236.

17. Akyürek O and Suksawang N. Vibration control by active integrated control system under bidirectional ground motions. *Adv Struct Eng* 2020; 2020: 596–610.

18. Malhotra PK. Response of buildings to near-field pulse-like ground motions. *Earthquake Eng Structural Dyn* 1999; 28(11): 1309–1326.

19. Mazza M. Effects of near-fault ground motions on the nonlinear behavior of reinforced concrete framed buildings. *Earthquake Sci* 2015; 28(4): 285–302.

20. Ghowsi AF and Sahoo DR. Seismic response of SMA-based self-centering buckling-restrained braced frames under near-fault ground motions. *Soil Dyn Earthquake Eng* 2020; 139: 106397.

21. Ghowsi AF and Sahoo DR. Near-field earthquake performance of SC-BRBs with optimal design parameters of SMA. *J Constructional Steel Res* 2020; 175: 106321.

22. Gentile R and Galasso C. Accounting for directivity-induced pulse-like ground motions in building portfolio loss assessment. *Bull Earthquake Eng* 2020; 19: 1–26.

23. Li H, Maghareh A, Montoya H, et al. Sliding mode control design for the benchmark problem in real-time hybrid simulation. *Mech Syst Signal Process* 2021; 151: 107364.

24. Liu Y, Kuang JS, and Yuen TY. Modal-based ground motion selection procedure for nonlinear response time history analysis of high-rise buildings. *Earthquake Eng Struct Dyn* 2020; 49(1): 95–110.

25. Zhang R, Wang D, Chen X, et al. Weighted and unweighted scaling methods for ground motion selection in time-history analysis of structures. *J Earthquake Eng* 2020; 26: 1–36.

26. Sigurðsson GÖ, Rupakhety R, Rahimi SE, et al. Effect of pulse-like near-fault ground motions on utility-scale land-based wind turbines. *Bull Earthquake Eng* 2020; 18(3): 953–968.

27. Ohtori Y, Christenson RE, Spencer BF, et al. Benchmark control problems for seismically excited nonlinear buildings. *J Eng Mech* 2004; 130(4): 366–385.

28. Wongprasert N and Symans MD. Application of a genetic algorithm for optimal damper distribution within the nonlinear seismic benchmark building. *J Eng Mech* 2004; 130(4): 401–406.

29. Ozbulut OE and Hurlebaus S. Application of an SMA-based hybrid control device to 20-story nonlinear benchmark building. *Earthquake Eng Struct Dyn* 2012; 41(13): 1831–1843.

30. Elias S and Matsagar V. Seismic vulnerability of a non-linear building with distributed multiple tuned vibration absorbers. *Struct Infrastructure Eng* 2019; 15(8): 1103–1118.

31. Elias S, Rupakhety R, and Ólafsson S. Tuned mass dampers for response reduction of a reinforced concrete chimney under near-fault pulse-like ground motions. In *Recent Advances and Applications of Seismic Isolation and Energy Dissipation Devices*. 2020.